Analytic G_0W_0 gradients based on a double-similarity transformation equation-of-motion coupled-cluster treatment

Marios-Petros Kitsaras, 1, a) Johannes Tölle, 2, b) and Pierre-François Loos 1, c)

The accurate prediction of ionization potentials (IPs) is central to understanding molecular reactivity, redox behavior, and spectroscopic properties. While vertical IPs can be accessed directly from electronic excitations at fixed nuclear geometries, the computation of adiabatic IPs requires nuclear gradients of the ionized states, posing a major theoretical and computational challenge, especially within correlated frameworks. Among the most promising approaches for IP calculations is the many-body Green's function *GW* method, which provides a balanced compromise between accuracy and computational efficiency. Furthermore, it is applicable to both finite and extended systems. Recent work has established formal connections between *GW* and coupled-cluster doubles (CCD) theory, leading to the first derivation of analytic *GW* nuclear gradients via a unitary CCD framework. In this work, we present an alternative, fully analytic formulation of *GW* nuclear gradients based on a modified version of the traditional equation-of-motion CCD formalism, enabling the inclusion of missing correlation effects in the traditional CCD methods.

I. INTRODUCTION

The ionization potential (IP) of a molecule, defined as the minimum energy required to remove an electron from a neutral species in its ground state, is a fundamental property that governs its reactivity, redox behavior, and spectroscopic signatures. Two main types of IPs are commonly distinguished: the vertical ionization potential (VIP) and the adiabatic ionization potential (AIP). These differ in whether or not nuclear relaxation of the ionic state is considered.

The VIP refers to the energy required to remove an electron without allowing the nuclei to move. In other words, the ionized state is constrained to the equilibrium geometry of the neutral molecule. This vertical transition approximates the Franck–Condon principle and is representative of ultrafast ionization events, where the nuclei remain effectively frozen during the electronic transition. Experimentally, VIPs manifest as sharp, intense peaks in photoelectron spectroscopy (PES), particularly when probed using ultraviolet or X-ray photons for valence and core levels, respectively.

In contrast, the AIP accounts for full nuclear relaxation in both the neutral and ionized states. It represents the true thermodynamic threshold for ionization, corresponding to the energy difference between the neutral ground state and the fully relaxed ionic ground state. As such, AIPs are directly linked to gas-phase thermochemistry and redox potentials. In PES experiments, AIPs appear as the onset of a given ionization band, while the corresponding VIP aligns with the maximum of the corresponding band. High-resolution PES, and in particular threshold photoelectron spectroscopy (TPES), are capable of resolving this onset with sufficient precision to extract both AIP and VIP from a single measurement.

The energy difference between VIP and AIP, known as the relaxation energy, provides insight into the structural reorga-

nization of the molecule upon ionization. A large relaxation energy indicates a significant geometric change, whereas a small value suggests that the neutral and ionic states share similar geometries. The simultaneous analysis of AIP and VIP in high-resolution PES thus enables a detailed understanding of the interplay between electronic structure and nuclear dynamics during ionization.

From a theoretical standpoint, the evaluation of VIPs is relatively straightforward. It requires knowledge of the ground-state equilibrium geometry and the ability to compute total energies of the neutral and cationic species at this fixed geometry. This can be achieved using standard electronic structure methods or, more efficiently, by computing excitation energies corresponding to electron removal (i.e., ionization) from the reference neutral ground state.

In contrast, the calculation of AIPs is more demanding, as it involves geometry optimization of the ionized species. This requires access to nuclear gradients of the ionized state, i.e., the first derivatives of the cationic energy with respect to the nuclear coordinates. Unlike ground-state gradients, which are routinely available in most quantum chemistry packages, ^{2–5} analytic gradients for charged excited states are significantly more challenging to derive and implement, ⁶ especially within correlated or many-body frameworks. ^{7–10} Nonetheless, these gradients are essential to perform geometry optimization, typically using a Newton-Raphson procedure, until a stationary point corresponding to the relaxed ionic minimum is reached.

While various computational approaches exist for accessing charged excitations, ranging from state-specific (e.g., ΔSCF) to equation-of-motion/linear-response formalisms, ^{11,12} one particularly promising method is the *GW* approximation ^{13–17} from many-body Green's function theory. ^{18,19} The *GW* formalism provides a robust framework to compute IPs^{20–33} and electron affinities (EAs)^{20–22,34–37} by approximating Hedin's equations. ^{13,38} It gained popularity due to its favorable balance between accuracy and computational cost. Its results often rival those of high-level wavefunction-based approaches, while remaining applicable to much larger molecular systems^{28,33,39–55} and, importantly, periodic materials. ^{18,19} Although traditionally

¹⁾Laboratoire de Chimie et Physique Quantiques (UMR 5626), Université de Toulouse, CNRS, Toulouse, France

²⁾Department of Chemistry, University of Hamburg, 22761 Hamburg, Germany; The Hamburg Centre for Ultrafast Imaging (CUI), Hamburg 22761, Germany

^{a)}Electronic mail: kitsaras@irsamc.ups-tlse.fr

b) Electronic mail: johannes.toelle@uni-hamburg.de

c)Electronic mail: loos@irsamc.ups-tlse.fr

limited to finite systems, equation-of-motion coupled-cluster (EOM-CC) has very recently been extended to periodic systems as well, using both Gaussian and plane-wave basis sets. 56,57

Recently, based on the established theoretical connections $^{58-60}$ between GW and coupled-cluster doubles (CCD) theory, $^{61-66}$ Tölle derived and implemented the first fully analytic GW nuclear gradients 67 (see also Refs. $^{68-73}$). His work has subsequently been extended to the first fully analytic Bethe-Salpeter equation (BSE) 74,75 nuclear gradients, $^{76-83}$ effectively generalizing the present formalism to neutral (optical) excited states. 84,85 These pioneering results exploit theoretical connections between GW and the unitary CCD (UCCD) $^{86-92}$ framework. 60 However, this approach necessitates the numerical evaluation of an infinite series of nested (anti)commutators, which is a non-standard numerical technique in traditional CCD implementations.

It would be, therefore, desirable to reformulate the GW nuclear gradients to leverage the well-established traditional EOM-CCD framework, as well as its extension to analytic properties. Unfortunately, a direct application of the traditional EOM-CCD formalism to GW is hindered by the missing correlation effects, as analyzed in detail in Refs. 60 and 93. In this work, we demonstrate how this obstacle can be overcome by introducing a modified version of the traditional EOM-CCD formalism, which we refer to as IP/EA-EOM- λ -direct-ring CCD. This approach allows (i) for the inclusion of missing correlation effects, and (ii) the derivation of analytic GW nuclear gradients within a more standard CC Lagrangian framework.

II. THEORY

A. The GW approximation

Similar to other Green's function approaches, the GW one-body Green's function G is expressed using the recursive Dyson equation

$$G = G_0 + G_0 \Sigma G. \tag{1}$$

The mean-field reference one-body Green's function G_0 , which for the current study corresponds to the Hartree-Fock (HF) approximation, is given by

$$G_0(\mathbf{x}_1\mathbf{x}_2;\omega) = \sum_i \frac{\phi_i^*(\mathbf{x}_1)\phi_i(\mathbf{x}_2)}{\omega - \epsilon_i^{\mathrm{HF}}} + \sum_a \frac{\phi_a^*(\mathbf{x}_1)\phi_a(\mathbf{x}_2)}{\omega - \epsilon_a^{\mathrm{HF}}}, \quad (2)$$

where $\phi_p(\mathbf{x})$ and ϵ_p^{HF} are the canonical HF orbitals and their corresponding energies. Likewise, the exact one-body Green's function is expressed as

$$G(\mathbf{x}_1 \mathbf{x}_2; \omega) = \sum_{I} \frac{\psi_I^*(\mathbf{x}_1)\psi_I(\mathbf{x}_2)}{\omega - \epsilon_I} + \sum_{A} \frac{\psi_A^*(\mathbf{x}_1)\psi_A(\mathbf{x}_2)}{\omega - \epsilon_A}, \quad (3)$$

where $\psi_I(x)$ and $\psi_A(x)$ are the so-called Dyson orbitals. The exact Green's function has poles at the energy differences associated with the electron-detached (hole states) and electron-attached (particle states) processes, namely, $\epsilon_I = E_0^N - E_I^{N-1}$

and $\epsilon_A = E_A^{N+1} - E_0^N$, where E_0^N is the ground-state energy of the neutral N-electron system, and E_I^{N-1} and E_A^{N+1} are the energies of the corresponding (N-1)- and (N+1)-electron states. Within the quasiparticle approximation, where only ionized and electron-attached states with a dominant single-particle character are retained, the Green's function reduces to the quasiparticle form

$$G(\mathbf{x}_1 \mathbf{x}_2; \omega) = \sum_i \frac{\psi_i^*(\mathbf{x}_1)\psi_i(\mathbf{x}_2)}{\omega - \epsilon_i} + \sum_a \frac{\psi_a^*(\mathbf{x}_1)\psi_a(\mathbf{x}_2)}{\omega - \epsilon_a}, \quad (4)$$

where ϵ_i and ϵ_a denote the hole and particle quasiparticle energies, respectively. In the following, the standard convention is used for the orbital indices, with i, j, k, \ldots denoting hole states, a, b, c, \ldots denoting particle states, and p, q, r, \ldots indicating either occupied or virtual orbitals.

The dynamical self-energy Σ describes correlation effects beyond the mean-field approximation. In GW, the self-energy is constructed using the dynamically-screened Coulomb interaction computed at the random-phase approximation (RPA) level of theory ^{94–100} and is given by

$$\Sigma_{pq}(\omega) = \sum_{i\mu} \frac{(pi|\mu)(\mu|qi)}{\omega - \epsilon_i + \Omega_{\mu}} + \sum_{a\mu} \frac{(ap|\mu)(\mu|aq)}{\omega - \epsilon_a - \Omega_{\mu}}.$$
 (5)

The quasiparticle energies and the effective two-electron integrals

$$(pq|\mu) = \sum_{ia} \left[\langle pa|qi \rangle \, x_{i,\mu}^a + \langle pi|qa \rangle \, y_{a,\mu}^i \right], \tag{6a}$$

$$(\mu|pq) = \sum_{ia} \left[\langle qi|pa \rangle \, x_{i,\mu}^{a*} + \langle qa|pi \rangle \, y_{a,\mu}^{i*} \right], \tag{6b}$$

are required to construct the elements of the self-energy. The index μ enumerates the solutions to the RPA problem where $x_{i,\mu}^a$ and $y_{a,\mu}^i$ are the elements of the eigenvector solutions corresponding to the excitation energy Ω_{μ} (see Sec. II B 1). The two-electron integrals $\langle pq|rs \rangle$ are given in Dirac notation i.e., $\langle 12|12 \rangle$.

By substituting Eqs. (2) and (5) into Eq. (1), one finds that the quasiparticle energies ϵ_p and corresponding Dyson orbitals $\psi_p(x)$ are obtained as the eigenvalues and eigenvectors of the following non-linear, frequency-dependent Fock-like operator:

$$\left[\hat{F} + \Sigma(\omega = \epsilon_p)\right] \psi_p(\mathbf{x}) = \epsilon_p \psi_p(\mathbf{x}). \tag{7}$$

 \hat{F} is the usual Fock operator including Hartree and exchange contributions, and the self-energy accounts for correlation effects. Although the so-called quasiparticle equation defined in Eq. (7) acts as the working equation for GW, its non-linear and dynamical nature makes it difficult to solve. In practice, it is solved iteratively due to the dependence of the self-energy on the quasiparticle energies [see Eq. (5)]. A hierarchy of approximations has been developed to address this issue, each defined by how the self-energy is constructed and updated at each iteration, leading to various levels of self-consistency (e.g., evGW, $^{101-105}$ qsGW, $^{50,106-112}$ etc.). Further details can be found in Ref. 17. The widely used G_0W_0 approximation corresponds to a single-shot calculation in which both the Green's

function and the screened interaction are fixed. ^{113–119} When combined with the diagonal approximation, the G_0W_0 quasiparticle energies are commonly obtained by solving the following one-dimensional, nonlinear equation for each state p:

$$\epsilon_p = \epsilon_p^{\rm HF} + \Sigma_{pp}(\omega = \epsilon_p).$$
 (8)

Green's function approaches are designed to describe properties of the many-body electronic state. In the case of G_0W_0 , the quasiparticle energies, associated with IPs in the hole space and EAs in the particle space, are improved relative to the mean-field reference. However, the total energy of the reference state is not uniquely defined. Various functionals have been proposed to calculate the correlation energy, including the Klein functional, 120 which is based on G, the Luttinger-Ward functional, $^{121-123}$ which is based on Σ , and the Galitskii-Migdal functional. 124,125 These expressions yield identical results only when a fully self-consistent Green's function (beyond the quasiparticle approximation) is used. 126-134 In other words, for nonself-consistent schemes such as G_0W_0 , they generally differ. Consequently, the total energy for the electron-detached or electron-attached state is also not uniquely defined within the G_0W_0 approximation. In the present work, the correlation energy of the ground state is evaluated at the RPA level (see Sec. IIB), which can be shown to be equivalent to the Klein functional.

By analogy with the extended Koopmans' theorem (EKT), in which the total energy of a charged state is approximated as

$$E_n^{\text{EKT}} = E_0^{\text{HF}} \mp \epsilon_n^{\text{HF}},\tag{9}$$

where $E_0^{\rm HF}$ is the HF energy of the reference state, we define the G_0W_0 total energy as

$$E_p^{G_0 W_0} = E_0^{G_0 W_0} \mp \epsilon_p^{G_0 W_0}, \tag{10}$$

where $E_0^{G_0W_0}$ consists of the mean-field HF energy and the RPA correlation energy, that is,

$$E_0^{G_0 W_0} = E_0^{HF} + E_c^{RPA}. (11)$$

Furthermore, Eq. (8) is not well-suited for deriving analytic derivatives. Unlike in standard Lagrangian formulations for non-variational ansätze, the identification of wavefunction parameters is obscured by the frequency dependence of the selfenergy. In this work, we derive a Lagrangian formulation that correctly reproduces the electronic energy of the charged states at the G_0W_0 level [see Eq. (10)]. This formulation exploits the connection between the RPA and a particular approximation to the CC expansion, as discussed in Sec. II B. Through this connection, an exact block-diagonalization of the RPA matrix is achieved. In Sec. IIC, this block-diagonalization is used to reformulate the nonlinear, frequency-dependent G_0W_0 problem into an EOM-CC problem. The resulting formalism not only provides a clear definition of the electron-detached (or -attached) energies, but also enables a standard Lagrangian construction for computing analytic derivatives.

B. Connection between RPA and drCCD

1. RPA

The RPA equations can be cast as a linear eigenvalue problem, $H_{\text{RPA}} \cdot R = R \cdot E$, that takes the form of Casida's equations ¹³⁵

$$\begin{pmatrix} A & B \\ -B^* & -A^* \end{pmatrix} \cdot \begin{pmatrix} X & Y^* \\ Y & X^* \end{pmatrix} = \begin{pmatrix} X & Y^* \\ Y & X^* \end{pmatrix} \cdot \begin{pmatrix} \Omega & \mathbf{0} \\ \mathbf{0} & -\Omega \end{pmatrix}, \tag{12}$$

where the elements of matrices A and B are given by

$$A_{ia,jb} = \langle \Phi_i^a | \hat{H} | \Phi_i^b \rangle, \tag{13a}$$

$$B_{ia,jb} = \langle \Phi_{ij}^{ab} | \hat{H} | \Phi_0 \rangle. \tag{13b}$$

The determinants $|\Phi_0\rangle$, $|\Phi_i^a\rangle$, $|\Phi_{ij}^{ab}\rangle$ are the reference, singly-and doubly-excited determinants constructed within the mean-field orbital space. The matrices \boldsymbol{X} and \boldsymbol{Y} are associated with single excitations and deexcitations, respectively, and gather the elements of the eigenvectors, $x_{i,\mu}^a$ and $y_{a,\mu}^i$ previously defined in Sec. II A. The diagonal matrix $\boldsymbol{\Omega}$ contains the positive excitation energy eigenvalues Ω_{μ} .

For the purposes of the GW approximation, the so-called direct version of RPA is considered. This approximation only affects the two-electron part of the normal-ordered Hamiltonian $\hat{H}_{\rm N} = \hat{F}_{\rm N} + \hat{V}_{\rm N}$, with $\hat{F}_{\rm N} = \sum_{pq} f_{pq} \{a_p^{\dagger} a_q\}$ the normal-ordered Fock operator. Specifically, the exchange contribution in the fluctuation potential,

$$\hat{V}_{N} = \frac{1}{4} \sum_{pqrs} \langle pq | | rs \rangle \{ a_{p}^{\dagger} a_{q}^{\dagger} a_{s} a_{r} \}$$

$$= \frac{1}{4} \sum_{pqrs} (\langle pq | rs \rangle - \langle pq | sr \rangle) \{ a_{p}^{\dagger} a_{q}^{\dagger} a_{s} a_{r} \},$$
(14)

is neglected. In this form, only the direct (Coulomb) component of the electron-electron interaction is retained, while the exchange term is omitted, consistent with the assumptions underlying the GW and direct RPA formalisms. Operators a_p^{\dagger} and a_p are the usual fermionic creators and annihilators, respectively, and the curly braces denote normal ordering with respect to the Fermi vacuum. Under this approximation, the matrix elements defined in Eq. (13) reduce to

$$A_{ia,jb} = \left(\epsilon_a^{\rm HF} - \epsilon_i^{\rm HF}\right) \delta_{ij} \delta_{ab} + \langle aj|ib\rangle, \qquad (15a)$$

$$B_{ia.ib} = \langle ab|ij\rangle, \tag{15b}$$

and the direct RPA correlation energy is given by the plasmon (or trace) formula: 98,136–138

$$E_{\rm c}^{\rm RPA} = \frac{1}{2} \left[\sum_{\mu} \Omega_{\mu} - \text{Tr}(A) \right]. \tag{16}$$

In the remainder of the manuscript, we will drop the term "direct" when referring to RPA, as it is always implied.

2. drCCD

It has been previously shown that RPA is equivalent to the direct-ring (dr) CCD (drCCD) truncation. 93,139–144 This approach constitutes an approximation to standard CCD, where the cluster operator includes all double excitations

$$\hat{T}_2 = \frac{1}{4} \sum_{ijab} t_{ij}^{ab} a_a^{\dagger} a_b^{\dagger} a_j a_i.$$
 (17)

Within the "ring" approximation, only those terms of the similarity-transformed Hamiltonian that correspond to loop (ring) diagrams are retained. It is well known that the ring approximation comes at the cost of breaking the fundamental antisymmetry of the electronic wavefunction. A bosonic character is introduced to a fundamentally fermionic system, and certain contractions among individual fermionic particle operators are ignored. As a result, the wavefunction fails to remain fully antisymmetric under electron exchange. In addition, only the direct Coulomb contribution of the fluctuation potential contributes, that is, excluding exchange. A modified set of rules for computing the drCCD Hamiltonian

$$\widetilde{H}_{\text{CCD}} = e^{-\hat{T}_2} \hat{H}_{\text{N}} e^{\hat{T}_2} \approx \widetilde{H}_{\text{dr}}$$
 (18)

using diagrammatic techniques is presented in Appendix A.

The drCCD amplitudes equations are given by projections of the drCCD Hamiltonian onto doubly-excited determinants

$$\langle \Phi_{ij}^{ab} | \widetilde{H}_{dr} | \Phi_0 \rangle \stackrel{!}{=} 0$$

$$\mathbf{B} + \mathbf{A} \cdot \mathbf{t} + \mathbf{t} \cdot \mathbf{A}^* + \mathbf{t} \cdot \mathbf{B}^* \cdot \mathbf{t} = \mathbf{0}.$$
(19)

The matrix t collects the drCCD amplitudes $t_{ia,jb} = t_{ij}^{ab}$. Within a standard CCD treatment, the correlation energy is given by

$$\begin{split} E_{\rm c}^{\rm CCD} &= \langle \Phi_0 | \, \widetilde{H}_{\rm CCD} \, | \Phi_0 \rangle \\ &= \frac{1}{4} \sum_{ijab} t_{ij}^{ab} \, \langle ij| \, |ab \rangle \\ &= \frac{1}{2} \sum_{ijab} t_{ij}^{ab} \, \langle ij| ab \rangle \,, \end{split} \tag{20}$$

where the antisymmetric form of the CCD amplitudes $(t_{ij}^{ab} = -t_{ji}^{ab} = t_{ji}^{ba})$ has been exploited. Applying the direct treatment within drCCD (where the amplitudes are not antisymmetric) is equivalent to using the last line of Eq. (20) for the correlation energy expression¹⁴⁰

$$E_{c}^{drCCD} = \langle \Phi_{0} | \widetilde{H}_{dr} | \Phi_{0} \rangle$$

$$= \frac{1}{2} \sum_{ijab} t_{ij}^{ab} \langle ij | ab \rangle$$

$$= \frac{1}{2} \operatorname{Tr}(\boldsymbol{B}^{*} \cdot \boldsymbol{t}).$$
(21)

Thus, an effective factor of 2 arises in the calculation of the expectation values of the drCCD Hamiltonian.

It can be further shown¹⁴⁰ that the drCCD correlation energy coincides with the RPA correlation energy

$$E_{\rm c}^{\rm drCCD} = E_{\rm c}^{\rm RPA}.$$
 (22)

The latter becomes apparent when the term $\sum_{\mu} \Omega_{\mu}$ in Eq. (16) is rewritten as the trace of a block-diagonal RPA matrix, as seen below in Eq. (40).

In order to obtain analytic derivatives of the RPA correlation energy, which is part of the total G_0W_0 electronic energy [see Eq. (10)], the method of Lagrange multipliers is employed. ^{145,146} Using the established connection to the dr-CCD approximation, ¹⁴⁷ the corresponding Lagrangian is defined as

$$\mathcal{L}_{c}^{drCCD} = \langle \Phi_{0} | \left(1 + \hat{\Lambda}_{2} \right) \widetilde{H}_{dr} | \Phi_{0} \rangle, \qquad (23)$$

with the λ -amplitude equations obtained by enforcing the following stationarity conditions

$$\frac{\partial \mathcal{L}_{c}^{drCCD}}{\partial t_{ij}^{ab}} = \langle \Phi_{0} | \left(1 + \hat{\Lambda}_{2} \right) \frac{\partial \widetilde{H}_{dr}}{\partial t_{ij}^{ab}} | \Phi_{0} \rangle \stackrel{!}{=} 0.$$
 (24)

The deexcitation operator $\hat{\Lambda}_2$ is given by

$$\hat{\Lambda}_2 = \frac{1}{4} \sum_{abij} \lambda_{ab}^{ij} a_i^{\dagger} a_j^{\dagger} a_b a_a. \tag{25}$$

The λ Lagrange multipliers can also be viewed as wavefunction parameters of the CC bra state within the bivariational formulation of CC.^{148–150} Eq. (24) can then be recast in matrix form as:

$$B^* + \lambda \cdot (A + A^* + B^* \cdot t + t \cdot B^*) = 0.$$
 (26)

The λ amplitude equations are linear in λ , which collects the elements of the λ amplitudes as $\lambda_{ia,jb} = \lambda_{ab}^{ij}$. A diagrammatic derivation accompanied by working equations can be found in Appendix B.

3. Block diagonalization of the RPA Hamiltonian

Previously, it has been shown that the exact correspondence between G_0W_0 and EOM-CC requires the block diagonalization of the RPA matrix⁶⁰

$$U^{\dagger} \cdot H_{\text{RPA}} \cdot U = \begin{pmatrix} \tilde{A} & \mathbf{0} \\ \mathbf{0} & -\tilde{A}^* \end{pmatrix}. \tag{27}$$

This can be achieved either through a Bogoliubov transformation or through an alternative unitary transformation, e.g., a unitary drCCD (drUCCD) treatment. ⁶⁰ In contrast, the *similarity-transformed* drCCD Hamiltonian is not equivalent to a *unitary transformation* even if it manages to reproduce the correlation energy $E_{\rm c}^{\rm RPA}$. The differences stem from the fact that the similarity transformation only treats the excitation part of Eq. (12) and does not fully account for both forward- and backward-time-ordered bubble diagrams present in GW, as first discussed in Ref. 58.

More precisely, the drCCD Hamiltonian corresponds to the following treatment of the RPA matrix

$$\bar{\boldsymbol{H}}_{\text{RPA}} = \boldsymbol{M}^{-1} \cdot \boldsymbol{H}_{\text{RPA}} \cdot \boldsymbol{M}, \tag{28}$$

with

$$\mathbf{M} = \begin{pmatrix} \mathbf{1} & t \\ \mathbf{0} & \mathbf{1} \end{pmatrix}, \qquad \mathbf{M}^{-1} = \begin{pmatrix} \mathbf{1} & -t \\ \mathbf{0} & \mathbf{1} \end{pmatrix}. \tag{29}$$

This transformation leads to a new eigenvalue equation of the form $\bar{H}_{RPA} \cdot \bar{R} = \bar{R} \cdot E$ with

$$\bar{\boldsymbol{H}}_{\text{RPA}} = \begin{pmatrix} \boldsymbol{A} + \boldsymbol{t} \cdot \boldsymbol{B}^* & \boldsymbol{B} + \boldsymbol{A} \cdot \boldsymbol{t} + \boldsymbol{t} \cdot \boldsymbol{A}^* + \boldsymbol{t} \cdot \boldsymbol{B}^* \cdot \boldsymbol{t} \\ -\boldsymbol{B}^* & -\boldsymbol{B}^* \cdot \boldsymbol{t} - \boldsymbol{A}^* \end{pmatrix}
= \begin{pmatrix} \boldsymbol{A} + \boldsymbol{t} \cdot \boldsymbol{B}^* & \boldsymbol{0} \\ -\boldsymbol{B}^* & -\boldsymbol{B}^* \cdot \boldsymbol{t} - \boldsymbol{A}^* \end{pmatrix},$$
(30)

and

$$\bar{R} = M^{-1} \cdot R = \begin{pmatrix} X - t \cdot Y & Y^* - t \cdot X^* \\ Y & X^* \end{pmatrix} = \begin{pmatrix} \bar{X} & \mathbf{0} \\ Y & X^* \end{pmatrix}, \quad (31)$$

where $\bar{X} = X - t \cdot Y$. The upper right block of \bar{H}_{RPA} vanishes as it represents the drCCD amplitude equations given by Eq. (19). Additionally, it can be shown that

$$t = Y^* \cdot X^{-1^*}. \tag{32}$$

We note that the formulation presented here to connect RPA to drCCD differs from those found in the literature by a complex conjugation. 93,140,142 Specifically, other works introduce the following parametrization

$$T = Y \cdot X^{-1} \tag{33}$$

as a first step to block-diagonalize the RPA matrix. The resulting matrix T corresponds to the deexcitation operator \hat{T}_2^{\dagger} rather than the excitation operator \hat{T}_2 [see Eq. (17)]. Numerical differences between the common derivation [see Eq. (33)] and Eq. (32) arise only when complex orbitals are employed, as the two formulations differ only in a complex conjugation. This is the case, for example, in the presence of a magnetic field as used in Ref. 151. Formally, however, the current derivation is consistent in defining the \hat{T}_2 as an excitation operator and not as a deexcitation operator.

In order to account for the contributions necessary to replicate the block diagonal structure of Eq. (28), a second similarity transformation is introduced

$$\bar{\boldsymbol{M}} = \begin{pmatrix} \mathbf{1} & \mathbf{0} \\ \lambda & \mathbf{1} \end{pmatrix}, \qquad \bar{\boldsymbol{M}}^{-1} = \begin{pmatrix} \mathbf{1} & \mathbf{0} \\ -\lambda & \mathbf{1} \end{pmatrix}. \tag{34}$$

The transformed problem reads $\widetilde{H}_{RPA} \cdot \widetilde{R} = \widetilde{R} \cdot E$ with

$$\widetilde{\boldsymbol{H}}_{RPA} = \overline{\boldsymbol{M}}^{-1} \cdot \overline{\boldsymbol{H}}_{RPA} \cdot \overline{\boldsymbol{M}}$$

$$= \begin{pmatrix} \boldsymbol{A} + \boldsymbol{t} \cdot \boldsymbol{B}^* & \boldsymbol{0} \\ -\left[\boldsymbol{B}^* + \boldsymbol{\lambda} \cdot (\boldsymbol{A} + \boldsymbol{A}^* + \boldsymbol{B}^* \cdot \boldsymbol{t} + \boldsymbol{t} \cdot \boldsymbol{B}^*)\right] & -\boldsymbol{B}^* \cdot \boldsymbol{t} - \boldsymbol{A}^* \end{pmatrix},$$
(35)

and

$$\widetilde{R} = \overline{M}^{-1} \cdot \overline{R} = \begin{pmatrix} \overline{X} & \mathbf{0} \\ -\lambda \cdot \overline{X} + Y & X^* \end{pmatrix}. \tag{36}$$

The lower left block of Eq. (35) vanishes as it is simply the negative of the λ -amplitude equations given by Eq. (26). Accordingly, it can be shown that the λ amplitudes are connected to the RPA parameters using $\lambda = Y \cdot \bar{X}^{-1}$. The final form for the doubly similarity-transformed RPA matrix in a block-diagonal form is given by

$$\widetilde{\boldsymbol{H}}_{\text{RPA}} = \begin{pmatrix} \boldsymbol{A} + \boldsymbol{t} \cdot \boldsymbol{B}^* & \boldsymbol{0} \\ \boldsymbol{0} & -(\boldsymbol{A}^* + \boldsymbol{B}^* \cdot \boldsymbol{t}) \end{pmatrix}, \tag{37a}$$

$$\widetilde{R} = \begin{pmatrix} \overline{X} & \mathbf{0} \\ \mathbf{0} & X^* \end{pmatrix}. \tag{37b}$$

We note that the matrix A is Hermitian $(A^* = A^{\mathsf{T}}, \text{ where})$ the superscript $^{\mathsf{T}}$ denotes the transpose of the matrix) and the matrices B and t are symmetric $(B = B^{\mathsf{T}})$ and $t = t^{\mathsf{T}}$. The deexcitation block can thus be rewritten as

$$\mathbf{A}^* + \mathbf{B}^* \cdot \mathbf{t} = (\mathbf{A} + \mathbf{t} \cdot \mathbf{B}^*)^{\mathsf{T}}. \tag{38}$$

As a result, the similarity-transformed RPA problem can be recast in the form of an expectation value

$$\begin{pmatrix} X^* & \mathbf{0} \\ \mathbf{0} & \bar{X} \end{pmatrix}^{\mathsf{T}} \cdot \begin{pmatrix} A + t \cdot B^* & \mathbf{0} \\ \mathbf{0} & -(A + t \cdot B^*)^{\mathsf{T}} \end{pmatrix} \cdot \begin{pmatrix} \bar{X} & \mathbf{0} \\ \mathbf{0} & X^* \end{pmatrix} = \begin{pmatrix} \mathbf{\Omega} & \mathbf{0} \\ \mathbf{0} & -\mathbf{\Omega} \end{pmatrix}, \tag{39}$$

which can be further simplified to

$$X^{\dagger} \cdot (A + t \cdot B^*) \cdot \bar{X} = \Omega. \tag{40}$$

This equation demonstrates that \bar{X} is the right eigenvector of the transformed RPA problem corresponding to the left eigenvector X^{\dagger} , where the superscript † denotes the Hermitian conjugate.

This block-diagonalization reduces the dimensionality of the original RPA problem by eliminating the coupling between excitations and deexcitations. Additionally, it establishes an exact relationship between the original RPA eigenvectors, X and Y, the left and right eigenvectors, X and X of the resulting non-Hermitian matrix, and the drCCD parameters, Y and Y.

It should be noted that the second similarity transformation is only needed to fully block diagonalize the RPA matrix, but the RPA problem can be represented in a reduced dimensionality using only the drCCD amplitudes [see Eqs. (30) and (31)]. Specifically, Eq. (40) can be alternatively derived using an excitation-energy EOM-CC treatment. 93,144 An EOM-singles (EOM-S) ansatz is used on the drCCD Hamiltonian, which yields the following right and left eigenvalue problems

$$\langle \Phi_i^a | \left[\widetilde{H}_{dr}, \hat{R}_{1,\mu} \right] | \Phi_0 \rangle = \Omega_\mu \langle \Phi_i^a | \hat{R}_{1,\mu} | \Phi_0 \rangle, \quad (41a)$$

$$\langle \Phi_0 | \hat{L}_{1,\mu} (\widetilde{H}_{dr} - E_c^{drCCD}) | \Phi_i^a \rangle = \langle \Phi_0 | \hat{L}_{1,\mu} | \Phi_i^a \rangle \Omega_{\mu}. \tag{41b}$$

These can be rewritten in matrix form as

$$(\mathbf{A} + \mathbf{t} \cdot \mathbf{B}^*) \cdot \mathbf{R}_1 = \mathbf{R}_1 \cdot \mathbf{\Omega}, \tag{42a}$$

$$\boldsymbol{L}_1 \cdot (\boldsymbol{A} + \boldsymbol{t} \cdot \boldsymbol{B}^*) = \boldsymbol{\Omega} \cdot \boldsymbol{L}_1. \tag{42b}$$

In this way, the right-EOM operator, $\hat{R}_{1,\mu} = \sum_{ia} r_{i,\mu}^a a_a^\dagger a_i$, can be identified to the matrix \bar{X} , and the left-EOM operator, $\hat{L}_{1,\mu} = \sum_{ia} l_{a,\mu}^i a_i^\dagger a_a$, to the matrix X^\dagger . Note that the parametrization in Eq. (32) directly influences the identification of the EOM eigenvectors to the RPA parameters. Previous formulations in the literature 93,144 are unclear whether \hat{T}_2^\dagger is used instead of \hat{T}_2 . This hinders the correct identification of left and right eigenvectors, and numerical differences are not limited to a complex conjugation. Specifically, the right-EOM vector is associated with X instead of \bar{X} and the other way around for the left-EOM vector, when \hat{T}_2^\dagger is employed.

C. G_0W_0 through the EOM-CC lens

As we shall discuss in detail in a forthcoming publication, the double similarity transformation described in Sec. II B 3 corresponds to the direct-ring approximation of an extended coupled-cluster doubles (ECCD) treatment ^{152–155}

$$\widetilde{H}_{\text{ECCD}} = e^{\hat{\Lambda}_2} e^{-\hat{T}_2} \hat{H}_{\text{N}} e^{\hat{T}_2} e^{-\hat{\Lambda}_2}. \tag{43}$$

The resulting approximated Hamiltonian, referred to here as the λ -drCCD transformation, is given by

$$\widetilde{H}_{\text{ECCD}} \approx \widetilde{H}_{\lambda\text{-dr}} = \widetilde{H}_{\text{dr}} + \left[\hat{\Lambda}_2, \widetilde{H}_{\text{dr}}\right],$$
 (44)

where the second similarity-transformation truncates exactly after the first-order commutator within the direct-ring approximation. The λ -direct-ring transformation includes all deexcitations (i.e., backward time-ordered bubble diagrams) that are missing in the standard drCCD similarity transformation compared to a unitary transformation, as discussed in Sec. II B 3.

1. The IP/EA-EOM-λ-drCCD expectation value

It has been shown that the quasiparticle equation [see Eq. (8)] can be recast as an eigenvalue problem resulting from an IP/EA equation-of-motion (IP/EA-EOM) approach acting on a block-diagonalized Hamiltonian, as mentioned in Sec. II B $3.^{59,156}$ Here, we make use of $\widetilde{H}_{\lambda\text{-dr}}$, as defined in Eq. (44). Specifically, the excitation space is chosen as the singles and doubles IP excitations (i.e., 1h and 2h1p, respectively) and EA deexcitations (i.e., 1p and 2p1h, respectively)

$$\begin{split} \hat{R}^{\text{IP/EA}} &= \sum_{I} R_{I}^{\text{IP/EA}} \hat{c}_{I}^{\text{IP/EA}} = \sum_{I} R_{I}^{\text{IP}} \hat{c}_{I}^{\text{IP}} + \sum_{I} R_{I}^{\text{EA}} \left(\hat{c}_{I}^{\text{EA}} \right)^{\dagger} \\ &= R_{1}^{\text{IP}} \hat{c}_{1}^{\text{IP}} + R_{2}^{\text{IP}} \hat{c}_{2}^{\text{IP}} + R_{1}^{\text{EA}} \left(\hat{c}_{1}^{\text{EA}} \right)^{\dagger} + R_{2}^{\text{EA}} \left(\hat{c}_{2}^{\text{EA}} \right)^{\dagger} \\ &= \sum_{i} r_{i} a_{i} + \sum_{ijb} r_{ji}^{b} a_{b}^{\dagger} a_{j} a_{i} \\ &+ \sum_{a} r_{a} a_{a} + \sum_{ajb} r_{ba}^{j} a_{j}^{\dagger} a_{b} a_{a}. \end{split} \tag{45}$$

Here, the collective operator $\hat{c}_I^{\text{IP/EA}}$ correspond to either the IP excitation operator, \hat{c}_I^{IP} , or EA deexcitation operator, $\left(\hat{c}_I^{\text{EA}}\right)^{\dagger}$.

They create the determinants involved in the IP/EA-EOM formalism when acting on the reference determinant, $\hat{c}_I | \Phi_0 \rangle = | \Phi_I \rangle$, with

$$\{|\Phi_I\rangle\} = \{|\Phi_i\rangle, |\Phi^a\rangle, |\Phi_i^{ba}\rangle, |\Phi_{ii}^{b}\rangle\}. \tag{46}$$

In addition, the index pair bj in the doubles amplitudes r^b_{ji} and r^j_{ba} follows the ring approximation, whereas the remaining index does not. As a result, these indices are formally nonequivalent, in contrast to the standard EOM-CC formulation. The resulting right and left non-Hermitian eigenvalue problems read

$$\langle \Phi_{0} | \left[\hat{c}_{I}^{\text{IP/EA},\dagger}, \left[\widetilde{H}_{\lambda - \text{dr}}, \hat{R}^{\text{IP/EA}} \right] \right]_{+} | \Phi_{0} \rangle =$$

$$\epsilon^{\text{IP/EA}} \langle \Phi_{0} | \left[\hat{c}_{I}^{\text{IP/EA},\dagger}, \hat{R}^{\text{IP/EA}} \right]_{+} | \Phi_{0} \rangle$$
(47)

and

$$\begin{split} \langle \Phi_{0} | \left[\hat{L}^{\text{IP/EA}}, \left[\widetilde{H}_{\lambda \text{-dr}}, \hat{c}_{I}^{\text{IP/EA}} \right] \right]_{+} | \Phi_{0} \rangle = \\ \epsilon^{\text{IP/EA}} \langle \Phi_{0} | \left[\hat{L}^{\text{IP/EA}}, \hat{c}_{I}^{\text{IP/EA}} \right]_{+} | \Phi_{0} \rangle \,. \end{split} \tag{48}$$

The anticommutator is represented by $[\cdot, \cdot]_+$ and the eigenvalues by $\{\epsilon^{\text{IP/EA}}\}$.

The total energy of the electron-attached or -detached state is expressed as the sum of the HF reference energy and the correlation energy at the drCCD level, augmented by the corresponding quasiparticle energy:

$$E_p^{\rm IP/EA} = E_0^{\rm HF} + E_c^{\rm drCCD} \pm \epsilon^{\rm IP/EA}.$$
 (49)

This result follows naturally from the EOM-CC formalism and coincides exactly with the definition given in Eq. (10).

The eigenvalues can also be expressed in an expectationvalue form, as follows:

$$\epsilon^{\text{IP/EA}} = \langle \Phi_0 | \left[\hat{L}^{\text{IP/EA}}, \left[\widetilde{H}_{\lambda \text{-dr}}, \hat{R}^{\text{IP/EA}} \right] \right]_{\perp} | \Phi_0 \rangle.$$
(50)

By enforcing a decoupling in the 1h and 1p spaces, the EOM vector for the collective IP and EA singles block reduces to having only one non-zero component

$$\hat{R}_{1,p}^{\text{IP/EA}} \approx \sum_{q} r_q a_q \delta_{pq} = r_p a_p. \tag{51}$$

This treatment corresponds to the diagonal approximation of G_0W_0 . The index p explicitly enumerates the solution for clarity. Within this approximation, the G_0W_0 quasiparticle energies exactly correspond to the IP/EA-EOM eigenvalues as $\epsilon_p^{\rm IP/EA} = -\epsilon_p^{G_0W_0}$.

It is again noted that the use of \widetilde{H}_{dr} instead of $\widetilde{H}_{\lambda\text{-dr}}$ would not reproduce the G_0W_0 quasiparticle energies, as it omits certain contributions from the deexcitation space. These missing terms are recovered through the second similarity transformation involving the deexcitation operator $\hat{\Lambda}_2$, which effectively eliminates the remaining off-diagonal block of the RPA matrix.

Details regarding the working equations can be found in Appendix C. Additionally, exact relations between the G_0W_0 and IP/EOM- λ -drCCD parameters can be found in Appendix D.

2. The Lagrangian treatment of G_0W_0

To derive an analytic expression for the derivatives of the IP/EA-EOM eigenvalues, we introduce the following Lagrangian:

$$\mathcal{L}^{\text{IP/EA}} = \pm \langle \Phi_{0} | \left[\hat{L}^{\text{IP/EA}}, \left[\widetilde{H}_{\lambda - \text{dr}}, \hat{R}^{\text{IP/EA}} \right] \right]_{+} | \Phi_{0} \rangle$$

$$\mp \epsilon^{\text{IP/EA}} \left(\langle \Phi_{0} | \left[\hat{L}^{\text{IP/EA}}, \hat{R}^{\text{IP/EA}} \right]_{+} | \Phi_{0} \rangle - 1 \right)$$

$$+ \langle \Phi_{0} | \left(1 + \hat{Z}_{2} \right) \widetilde{H}_{\text{dr}} | \Phi_{0} \rangle$$

$$+ \langle \Phi_{0} | \left(1 + \hat{\Lambda}_{2} \right) \left[\widetilde{H}_{\text{dr}}, \hat{\Xi}_{2} \right] | \Phi_{0} \rangle,$$
(52)

which, by construction, reproduces the total correlation energy of the electron-detached or -attached state

$$E_{\rm c}^{\rm IP/EA} = E_{\rm c}^{\rm drCCD} \pm \epsilon^{\rm IP/EA}$$
 (53)

from Eq. (49). The reference correlation energy contribution is contained in the third term of the Lagrangian. Regarding the sign of the first term in the Lagrangian, the EOM expectation value is derived as an excitation, and, as such, is added for the IP case. For the EA case, on the other hand, the expectation value corresponds to a deexcitation and must be subtracted.

The Lagrange multipliers introduced in Eq. (52) are as follows: (i) the EOM eigenvalue $\epsilon^{\text{IP/EA}}$ enforces the biorthonormality condition between the left- and right-EOM vectors in the second term; (ii) the deexcitation operator

$$\hat{Z}_{2} = \frac{1}{4} \sum_{ijab} \zeta_{ab}^{ij} a_{i}^{\dagger} a_{j}^{\dagger} a_{b} a_{a}$$
 (54)

includes the drCCD-amplitude equations for \hat{T}_2 [see Eq. (19)] in the third term; and (iii) the excitation operator

$$\hat{\Xi}_{2} = \frac{1}{4} \sum_{ijab} \xi_{ij}^{ab} a_{a}^{\dagger} a_{b}^{\dagger} a_{j} a_{i}$$
 (55)

the λ -amplitude equations for $\hat{\Lambda}_2$ [see Eq. (24)] in the fourth term.

Enforcing the stationarity conditions on the Lagrangian [see Eq. (52)] results in the following set of equations:

1. Stationarity with respect to the Lagrange multipliers ζ_{ab}^{ij} ,

$$\frac{\partial \mathcal{L}^{\text{IP/EA}}}{\partial \zeta_{ab}^{ij}} \stackrel{!}{=} 0, \tag{56}$$

reproduces the pseudo-linear drCCD amplitude equations [see Eq. (19)].

2. Stationarity with respect to the Lagrange multipliers ξ_{ii}^{ab} ,

$$\frac{\partial \mathcal{L}^{\text{IP/EA}}}{\partial \xi_{ab}^{ij}} \stackrel{!}{=} 0, \tag{57}$$

reproduces the linear drCCD λ -amplitude equations [see Eq. (24)].

3. Stationarity with respect to the left-EOM amplitudes l_I ,

$$\frac{\partial \mathcal{L}^{\text{IP/EA}}}{\partial l_I} \stackrel{!}{=} 0, \tag{58}$$

reproduces the right eigenvalue problem [see Eq. (47)].

4. Stationarity with respect to the right-EOM amplitudes r_I ,

$$\frac{\partial \mathcal{L}^{\text{IP/EA}}}{\partial r_I} \stackrel{!}{=} 0, \tag{59}$$

reproduces the left eigenvalue problem [Eq. (48)].

5. Stationarity with respect to the Lagrange multiplier $\epsilon^{\text{IP/EA}}$,

$$\frac{\partial \mathcal{L}^{\text{IP/EA}}}{\partial \epsilon^{\text{IP/EA}}} \stackrel{!}{=} 0, \tag{60}$$

reproduces the biorthonormality condition

$$\langle \Phi_0 | \left[\hat{L}^{\text{IP/EA}}, \hat{R}^{\text{IP/EA}} \right]_+ | \Phi_0 \rangle = 1. \tag{61}$$

6. Stationarity with respect to the λ -amplitudes,

$$\frac{\partial \mathcal{L}^{\text{IP/EA}}}{\partial \lambda_{ab}^{ij}} \stackrel{!}{=} 0, \tag{62}$$

yields the inhomogeneous linear ξ amplitude equations

$$\begin{split} \mp \langle \Phi_{0} | \left[\hat{L}^{\text{IP/EA}}, \left[\frac{\partial \widetilde{H}_{\lambda\text{-dr}}}{\partial \lambda_{ab}^{ij}}, \hat{R}^{\text{IP/EA}} \right] \right]_{+} | \Phi_{0} \rangle = \\ \langle \Phi_{ij}^{ab} | \left[\widetilde{H}_{\text{dr}}, \hat{\Xi}_{2} \right] | \Phi_{0} \rangle \,. \end{split} \tag{63}$$

7. Stationarity with respect to the drCCD amplitudes

$$\frac{\partial \mathcal{L}^{\text{IP/EA}}}{\partial t_{ij}^{ab}} \stackrel{!}{=} 0 \tag{64}$$

yields the inhomogeneous linear ζ amplitude equations

$$\mp \langle \Phi_0 | \left[\hat{L}^{\text{IP/EA}}, \left[\frac{\partial \widetilde{H}_{\lambda - \text{dr}}}{\partial t_{ij}^{ab}}, \hat{R}^{\text{IP/EA}} \right] \right]_+ |\Phi_0\rangle \\
- \langle \Phi_0 | \left(1 + \hat{\Lambda}_2 \right) \left[\frac{\partial \widetilde{H}_{\text{dr}}}{\partial t_{ij}^{ab}}, \hat{\Xi}_2 \right] |\Phi_0\rangle = \langle \Phi_0 | \left(1 + \hat{Z}_2 \right) \frac{\partial \widetilde{H}_{\text{dr}}}{\partial t_{ij}^{ab}} |\Phi_0\rangle .$$
(65)

Since Eq. (65) includes contributions from the ξ amplitudes, the set of linear equations in Eq. (63) has to be solved first, and is thus decoupled. The diagrammatic representation and the derivation of working equations are presented in Appendix C.

Compared to the drUCCD approach employed in Ref. 67, the λ -drCCD formulation avoids the need for a numerical

truncation of the otherwise non-terminating Baker-Campbell-Hausdorff (BCH) expansion inherent to the unitary CC framework. This advantage, however, comes at the cost of introducing additional sets of wavefunction parameters, namely, the left-EOM vector, the λ amplitudes, and the ξ amplitudes.

After recasting Eq. (52) as a function of the contributions of the one- and two-electron reduced density matrices,

$$\mathcal{L}^{\text{IP/EA}} = \sum_{pq} \gamma_{pq} f_{pq} + \frac{1}{2} \sum_{pqrs} \Gamma_{pqrs} \langle pq|rs \rangle, \qquad (66)$$

and a subsequent Hermitization, i.e.,

$$\bar{\mathcal{L}}^{\text{IP/EA}} = \frac{\mathcal{L}^{\text{IP/EA}} + (\mathcal{L}^{\text{IP/EA}})^*}{2},\tag{67}$$

to derive Hermitian reduced densities

$$\bar{\gamma}_{pq} = \frac{\gamma_{pq} + \gamma_{qp}^*}{2}, \qquad \bar{\Gamma}_{pqrs} = \frac{\Gamma_{pqrs} + \Gamma_{rspq}^*}{2}, \qquad (68)$$

the *z*-vector method can be applied to account for the orbital relaxation.² The resulting Lagrangian is

$$\mathcal{L}_{\text{rel}}^{\text{IP/EA}} = \bar{\mathcal{L}}^{\text{IP/EA}} + \sum_{pq} w_{pq} (f_{pq} - \delta_{pq} \epsilon_p) + \sum_{pq} I_{pq} (S_{pq} - \delta_{pq}).$$
(69)

The Lagrange multipliers w_{pq} and I_{pq} are introduced for the diagonal form of the Fock matrix and the orbital orthonormality $S_{pq} = \langle \phi_p | \phi_q \rangle = \delta_{pq}$, respectively. They can be assumed Hermitian with no loss of generality. The diagonal approximation that results in the decoupling of the singles-singles block in the EOM problem implies that the method is not invariant under rotations within the occupied-occupied and virtual-virtual orbital subspaces. As a consequence, the w_{pq} amplitudes acquire non-zero components in these blocks, even in the absence of a frozen-core approximation. Working equations for the evaluation of w_{pq} and I_{pq} are provided in Ref. 157.

Incorporating the w_{pq} contributions in the one-body reduced density matrix, $\gamma_{pq}^{\rm rel} = \bar{\gamma}_{pq} + w_{pq}$, yields a final expression for the derivative of the energy with respect to a parameter κ that depends only on the partial derivatives of the mean-field Fock matrix elements, the two-electron integrals, and the overlap integrals:

$$\begin{split} \frac{\mathrm{d}E^{\mathrm{IP/EA}}}{\mathrm{d}\kappa} &= \frac{\partial \mathcal{L}^{\mathrm{IP/EA}}}{\partial \kappa} \\ &= \sum_{pq} \gamma_{pq}^{\mathrm{rel}} \frac{\partial f_{pq}}{\partial \kappa} + \sum_{pq} I_{pq} \frac{\partial S_{pq}}{\partial \kappa} + \frac{1}{2} \sum_{pqrs} \bar{\Gamma}_{pqrs} \frac{\partial \langle pq|rs \rangle}{\partial \kappa}. \end{split} \tag{70}$$

Different choices for the parameter κ lead to expressing first-order properties as analytic first-order derivatives of the energy. In the case of κ being nuclear displacements, geometrical gradients are derived to use in a geometry optimization calculation.

III. COMPUTATIONAL DETAILS

For the purpose of the current work, the drCCD approximation (energy and fully analytic properties), and the G_0W_0

approximation through the IP/EA-EOM- λ -drCCD formulation (energy and fully analytic properties) were implemented in the QCUMBRE program package. ¹⁵⁸ The integrals and the SCF solution are provided by the MINT module ¹⁵⁹ of the CFOUR program package. ^{160,161} The geometry optimizer of CFOUR was also used to get the equilibrium geometries.

The verification of the RPA and G_0W_0 energies was achieved through comparison to the QUACK program package. ¹⁶² Analytic one-electron properties were tested in the case of dipole moments against numerical derivatives with finite electric-field calculations. Accordingly, analytic geometric gradients were tested against numerical differentiation by finite displacements of the nuclear coordinates, as well as the implementation reported in Ref. 67.

The implemented method was applied on the GW20 $set^{23,25,163}$ (composed by the 20 smallest systems of the GW100set²⁰) where the He, Ne, and Ar atomic systems were excluded. Results were generated in different levels of theory for comparison and benchmarking purposes. Specifically, the optimal geometry of the neutral system was calculated at the groundstate ADC(2), CC2, G_0W_0 , CCSD, and CC3 levels of theory. For the purposes of the current study, only closed-shell configurations were targeted, even if for some systems a triplet state may be lower in energy. To target the lowest electronic state of the cationic systems, calculations were performed at the excited-state ADC(2), EOM-CC2, G_0W_0 , EOM-CCSD, and EOM-CC3 levels of theory. For EOM-CCSD, the corresponding IP-EOM-CC implementation was used, while excitations in continuum orbitals were probed to target the respective cationic states in the case of ADC(2), EOM-CC2, and EOM-CC3. 164 All electrons were included for the calculation of correlation effects using the aug-cc-pVTZ basis set. 165-168 The scheme to generate G_0W_0 quasiparticle energies, as described in the previous paragraphs, corresponds to an η parameter of 0 on top of canonical restricted HF orbitals. In the following discussion, the RPA ground-state energy for the neutral system calculated via the drCCD scheme can be assumed when referring to G_0W_0 results.

All calculations were performed using the QCUMBRE 158 and CFOUR program packages. $^{159-161}$ A double convergence criterion of 10^{-7} $E_{\rm h}$ for the energy difference and 10^{-7} for the DIIS error was used for the HF calculation. Accordingly, a 10^{-7} criterion was used for the norm of the residual vector in the linear solver for the drCCD and λ amplitudes, and in the Davidson algorithm for the excited-state calculations. For the geometry optimizations, a convergence criterion of 10^{-6} $E_{\rm h}a_0^{-1}$ was used for the gradient norm in the quasi-Newton algorithm.

IV. RESULTS

In the following paragraphs, results regarding the closedshell states of the neutral systems and the corresponding lowest in energy states of the cationic systems in the molecular subset of the *GW*20 set are presented. Vertical IPs were calculated as the energy difference between the ionized-state and groundstate energy at the geometry optimized for the neutral system at the corresponding level of theory. Instead, for the calculation

TABLE I. Vertical and adiabatic ionization potentials (in eV) using the aug-cc-pVTZ basis set. The IRREP of the HOMO is reported. For the vertical IPs, the optimal geometry of the neutral molecule at the respective level of theory has been used. For the adiabatic IPs, the energy of the ionized state at the optimal geometry calculated at the respective level of theory has been subtracted from the optimal energy of the neutral molecule at the respective level of theory. The MAE and MSE are reported with respect to the IP-EOM-CC3 results.

		Vertical IPs			Adiabatic IPs						
System	HOMO	ADC(2)	CC2	G_0W_0	CCSD	CC3	ADC(2)	CC2	G_0W_0	CCSD	CC3
H_2	σ_g^+	16.350	16.330	18.036	16.397	16.397	15.415	15.387	15.621	15.520	15.520
LiH	σ^{+}	8.024	8.002	8.233	8.005	8.005	7.783	7.757	8.024	7.728	7.729
BH_3	e'	13.290	13.251	13.716	13.353	13.314	12.223	12.193	12.620	12.315	12.285
Li_2	$\sigma_g^{\scriptscriptstyle +}$	5.178	5.155	5.348	5.235	5.235	5.073	5.057	5.240	5.121	5.121
CH_4	t_2	14.115	14.056	14.797	14.404	14.369	12.490	12.428	13.110	12.825	12.758
NH_3	a'	10.185	10.163	11.162	10.857	10.891	9.441	9.416	10.414	10.121	10.135
H_2O	b_1	11.519	11.542	12.916	12.615	12.666	11.328	11.347	12.841	12.516	12.565
HF	π	14.643	14.719	16.273	16.045	16.132	14.320	14.389	16.154	15.896	15.976
BN	π	10.812	10.856	11.769	12.005	12.071	10.700	10.730	11.722	11.892	11.914
BeO	π	8.237	7.784	9.976	10.041	9.744	7.472	6.982	9.768	9.897	8.755
LiF	π	9.665	9.773	11.432	11.427	^b 11.391	8.785	a	10.965	10.980	^b 10.892
CO	$\sigma^{\scriptscriptstyle +}$	14.000	13.766	14.721	14.179	13.866	13.990	13.762	14.685	14.159	13.860
N_2	π_u	17.108	16.999	17.267	17.314	16.851	16.899	16.771	16.963	17.051	16.461
BF	$\sigma_g^{\scriptscriptstyle +}$	11.024	10.955	11.266	11.235	11.102	10.931	10.864	11.165	11.130	11.012
H_2S	b_1°	10.179	10.148	10.508	10.414	10.381	10.164	10.132	10.503	10.404	10.370
HCl	π	12.408	12.389	12.789	12.704	12.664	12.373	12.355	12.772	12.680	12.641
F_2	π_g	14.124	14.156	16.122	15.562	15.756	14.101	14.149	15.854	15.397	15.591
MAE		0.635	0.652	0.359	0.107		0.667	0.603	0.307	0.163	
MSE		-0.587	-0.635	0.323	0.056		-0.594	-0.561	0.284	0.120	

^a A geometry optimization for LiF⁺ at the IP-EOM-CC2 level was not possible due to the deteriorating quality of the reference CC2 wavefunction for interatomic distances near the expected optimal geometry for the LiF⁺ cation. In addition, the LiH results have been excluded when calculating the MAE and MSE in all cases due to apparent qualitative differences between the different levels of theory.

TABLE II. Interatomic distance (in \mathring{A}) in the optimal geometry for the neutral R_{neu} and cationic R_{cat} linear molecules using the aug-cc-pVTZ basis set. The MAE and MSE are reported with respect to the CC3 and IP-EOM-CC3 results.

			$R_{ m neu}$					$R_{\rm cat}$		
System	ADC(2)	CC2	G_0W_0	CCSD	CC3	ADC(2)	CC2	G_0W_0	CCSD	CC3
H_2	0.7374	0.7377	0.7354	0.7430	0.7430	1.0627	1.0657	1.0578	1.0581	1.0581
LiH	1.5879	1.5883	1.5719	1.5924	1.5922	2.0544	2.0599	1.9661	2.1635	2.1633
Li_2	2.7125	2.7117	2.6725	2.6623	2.6600	3.1636	3.1431	3.1278	3.1076	3.1030
HF	0.9201	0.9225	0.9097	0.9164	0.9196	1.0671	1.0753	0.9799	0.9989	1.0075
BN	1.3212	1.2972	1.2700	1.2713	1.2765	1.3691	1.3657	1.3058	1.3362	1.3489
BeO	1.3452	1.4101	1.3077	1.3200	1.3621	1.6012	1.6097	1.4026	1.3975	1.6061
LiF	1.5817	1.5880	1.5641	1.5722	^b 1.5762	2.7302	a	1.9711	1.9600	^b 2.0344
CO	1.1342	1.1442	1.1150	1.1241	1.1335	1.1203	1.1351	1.0923	1.1067	1.1234
N_2	1.1097	1.1167	1.0830	1.0929	1.1007	1.1712	1.1853	1.1489	1.1560	1.1869
BF	1.2640	1.2699	1.2521	1.2629	1.2686	1.2109	1.2163	1.1994	1.2075	1.2160
HCl	1.2710	1.2717	1.2649	1.2728	1.2751	1.3212	1.3222	1.2979	1.3138	1.3156
F_2	1.3977	1.4152	1.3641	1.3918	1.4137	1.3545	1.3872	1.2608	1.2997	1.3145
MAE	0.0137	0.0148	0.0196	0.0087		0.0853	0.0302	0.0597	0.0318	
MSE	0.0051	0.0127	-0.0176	-0.0083		0.0624	0.0111	-0.0556	-0.0310	

^a A geometry optimization for LiF⁺ at the IP-EOM-CC2 level was not possible due to the deteriorating quality of the reference CC2 wavefunction for interatomic distances near the expected optimal geometry for the LiF⁺ cation. In addition, the LiH results have been excluded when calculating the MAE and MSE in all cases due to apparent qualitative differences between the different levels of theory.

of the adiabatic IPs, the same ground-state energy was used in combination with the ionized-state energy calculated at the geometry optimized for the cationic system at the corresponding level of theory. The IPs are collected in Table I, where the irreducible representation (IRREP) of the highest occupied molecular orbital (HOMO) is also reported. In the present

^b Prediction at the IP-EOM-CC3 level for the LiF⁺ are non consistent. For this reason, predictions at the CCSDT level were used. Further details can be found in the Supplementary Material.

b Prediction at the IP-EOM-CC3 level for the LiF⁺ are non consistent. For this reason, predictions at the CCSDT level were used. Further details can be found in the Supplementary Material.

TABLE III. Geometric parameters in the optimal geometry for the neutral and cationic polyatomic molecules using the aug-cc-pVTZ basis set. Distances are given in Å and angles in °. The point group (PG) of the molecular symmetry is reported in the last column.

System	ADC(2)	CC2	G_0W_0	CCSD	CC3	Param.	PG
BH ₃	1.1811	1.1814	1.1756	1.1840	1.1848	R	\mathcal{D}_{3h} a
	1.4140	1.4096	1.4420	1.4395	1.4365	R_1	
BH_3^+	1.1749	1.1765	1.1636	1.1776	1.1801	R_2	$C_{2v}^{\mathbf{b}}$
	164.62	164.71	163.07	163.07	163.38	ω	
CH ₄	1.0841	1.0846	1.0808	1.0863	1.0879	R	$\mathcal{T}_d^{\mathbf{c}}$
	1.1760	1.1781	1.1746	1.1782	1.1838	R_1	
$\mathrm{CH_4}^+$	55.15	55.04	56.08	56.14	55.34	ω_1	$C_{2\nu}^{d}$
CH_4	1.0796	1.0812	1.0670	1.0783	1.0805	R_2	C_{2v}
	125.43	125.42	125.33	125.01	125.54	ω_2	
NH ₃	1.0095	1.0107	1.0024	1.0095	1.0122	R	$C_{3v}^{\mathbf{e}}$
-	111.80	111.94	111.49	111.90	112.15	ω	C_{3v}
NH ₃ ⁺	1.0275	1.0293	1.0068	1.0187	1.0209	R	$\mathcal{D}_{3h}^{\mathbf{f}}$
H ₂ O	0.9588	0.9607	0.9484	0.9561	0.9591	R	$C_{2v}^{\mathbf{g}}$
	104.27	104.06	105.01	104.59	104.33	ω	C_{2v}
H ₂ O ⁺	1.0245	1.0285	0.9798	0.9972	1.0009	R	C g
$\Pi_2 O$	108.73	108.20	110.59	109.38	109.38	ω	$C_{2v}^{\mathbf{g}}$
H_2S	1.3319	1.3326	1.3264	1.3351	1.3375	R	$C_{2\nu}^{\mathbf{h}}$
	91.93	91.87	92.51	92.27	92.00	ω	C_{2v}
H_2S^+	1.3558	1.3575	1.3394	1.3550	1.3579	R	C h
	92.69	92.63	93.29	92.99	92.71	ω	$C_{2v}^{\mathbf{h}}$

^a Planar symmetric. R is the B-H distance.

calculation, the lowest-energy cationic state consistently corresponds to removing an electron from the HOMO. In Tables II and III, the geometric parameters of the optimal geometries of the neutral and the cationic systems are presented. Intermolecular distances for diatomic molecules are reported in Table II. The point group (PG) of the neutral and cationic systems in the case of polyatomic molecules, accompanied by a description of the reported geometrical parameters, can be found in Table III. In Tables I and II, the mean absolute error (MAE) and mean signed error (MSE) have been calculated with respect to the CC3 and IP-EOM-CC3 results. The only exception is LiF for which we employed CCSDT reference values. This point is discussed in detail in the Supplementary Material.

Regarding the IPs (Table I), the relative performance of the methods remains essentially consistent between vertical and adiabatic values. ADC(2) and CC2 yield comparable results, with MAEs of approximately $0.6 \,\mathrm{eV}$ to $0.7 \,\mathrm{eV}$ and negative MSEs of similar magnitude. The G_0W_0 approximation performs noticeably better, producing MAEs in the range of

 $0.3\,\mathrm{eV}$ to $0.4\,\mathrm{eV}$ and positive MSEs of comparable size. Similar superior performance of G_0W_0 compared to ADC(2) has also been observed in Ref. 67 without employing the diagonal approximation as used in the current work. CCSD delivers the most accurate results, with small positive MSEs and MAEs between $0.1\,\mathrm{eV}$ to $0.2\,\mathrm{eV}$. The VIP of H_2 , however, is known to be poorly described, likely due to the self-screening problem inherent to the GW approximation. $^{169-172}$ In contrast, the AIP appears largely unaffected.

For the equilibrium geometries of the diatomic molecules (Table II), ADC(2), CC2, and CCSD all outperform G_0W_0 . While the errors in the ground-state bond lengths are generally small (0.01 Å to 0.02 Å), the deviations in the equilibrium geometries of the corresponding cations are larger by a factor of two to three for all methods. Consistent with observations for neutral excited states, 173,174 CCSD tends to underestimate bond lengths in the cationic states, whereas ADC(2) and CC2 systematically overestimate them. Similarly, G_0W_0 exhibits a systematic underestimation of cationic bond lengths, in contrast to BSE@ G_0W_0 , which has been shown to overestimate bond-length changes upon excitation in the case of neutral excitations. 83 Analogous trends are observed for the larger polyatomic species in the test set (Table III).

V. CONCLUSION

In this work, we have presented the implementation of the ionization-potential and electron-affinity equation-of-motion λ -direct-ring coupled-cluster doubles (IP/EA-EOM- λ -drCCD) formalism, enabling the computation of fully analytic G_0W_0 energies and nuclear gradients within a standard CC Lagrangian framework. The approach has been implemented in the QCUMBRE program package and rigorously verified against numerical derivatives, as well as existing analytic implementations of GW gradients. 67

Benchmark calculations were performed on the molecular subset of the GW20 test set. Both vertical and adiabatic IPs were obtained at various levels of theory and compared to CC3 and IP-EOM-CC3 reference data. The results confirm that the newly implemented G_0W_0 formalism yields IPs with MAEs in the range of $0.3 \, \text{eV}$ to $0.4 \, \text{eV}$, thereby outperforming second-order methods such as ADC(2) and CC2. The equilibrium geometries of both neutral and cationic species are accurately reproduced, with typical bond-length deviations on the order of $0.01 \, \text{Å}$ for neutrals and slightly larger discrepancies for cations. Systematic trends were observed across methods: CCSD and G_0W_0 tend to underestimate bond lengths in cationic states, whereas ADC(2) and CC2 systematically overestimate them.

These results demonstrate that the IP/EA-EOM- λ -drCCD formulation provides new route for obtaining fully analytic G_0W_0 properties, by leveraging the connection between Green's function and coupled-cluster theories. The achieved agreement with high-level wavefunction benchmarks highlights the accuracy and robustness of the approach, while its analytic nature opens the door to geometry optimization and property evaluation for larger and more complex systems. In future work, we plan to conduct a more extensive benchmark

^b Planar with one nonequivalent B – H bond. R_1 is the nonequivalent B – H distance, R_2 is the B – H distance of the equivalent H atomic centers, ω is the angle H – B – H angle between the equivalent H atomic centers.

^c Tetrahedral symmetric. *R* is the C–H distance.

^d Two pairs of equivalent H atomic centers. R_1 is the C-H distance of the first pair, ω_1 is the H-C-H angle of the first pair, R_2 is the C-H distance of the second pair, ω_2 is the H-C-H angle of the second pair.

^e R is the N-H distance and ω is the angle of the N-H with respect to the C_3 rotational axis.

f Planar symmetric. R is the N-H distance.

^g R is the O-H distance, ω is the H-O-H angle. The symmetry does not change between the neutral and cationic systems.

^h R is the S-H distance, ω is the H-S-H angle. The symmetry does not change between the neutral and cationic systems.

study on a broader set of IPs and EAs, in order to further assess the transferability and accuracy of the present formulation across diverse chemical environments. Extensions toward self-consistent *GW* variants and BSE within the same analytic formulation are also under active development.

ACKNOWLEDGMENTS

This project has received funding from the European Research Council (ERC) under the European Union's Horizon 2020 research and innovation programme (Grant agreement No. 863481). J. T. acknowledges funding from the Fonds der Chemischen Industrie (FCI) via a Liebig fellowship and support by the Cluster of Excellence "CUI: Advanced Imaging of Matter" of the Deutsche Forschungsgemeinschaft (DFG) (EXC 2056, funding ID 390715994). This work used the HPC resources from CALMIP (Toulouse) under allocation 2025-18005. M.-P. K. thanks Dr. Laura Grazioli for her support with generating the ADC(2) results.

DATA AVAILABILITY STATEMENT

The data that support the findings of this study are available within the article and its supplementary material.

APPENDICES

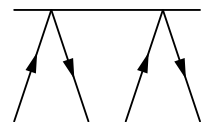
Appendix A: Diagrammatic rules for the direct-ring approximation and additional aspects

In the diagrammatic representation, we employ the following conventions and graphical elements.

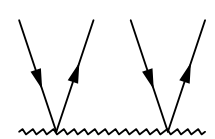
• Operator \hat{T}_2 :



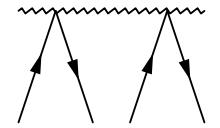
Operator Â₂:



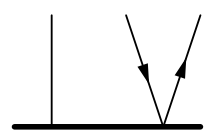
• Operator $\hat{\Xi}_2$:



• Operator \hat{Z}_2 :



• The left and right EOM operators, \hat{L} and \hat{R} , are depicted by bold lines, such as



• The Fock operator and the two-electron interaction are depicted by dashed lines, such as



• The vertices with open circles are used to denote the indices of the one- and two-body reduced density matrices. Lines connected to open circles are to be treated as external lines starting from the vertex. For example, γ_{ab} is depicted as



• Otherwise, the standard convention can be assumed. 63,66

In the direct ring approximation, the following rules are imposed in addition to the standard CC diagrammatic rules. 63,66

1. **Loop connectivity:** Indices subject to the ring approximation must connect the same initial and final vertices, i.e., they must form a closed loop:



The Fock operator is exempt from this rule.

2. **Symmetrization of non-equivalent external indices:** For external, non-equivalent indices obeying the ring approximation, symmetrization (but not antisymmetrization) is applied separately to each particle-particle or hole-hole index. For example, for two external index pairs *ia* and *jb*, the symmetrization is performed as

$$P(ia|jb)M_{ia\,ib} = M_{ia\,ib} + M_{ibia}. (A1)$$

Individual antisymmetrizations over occupied [P(ij)] or virtual [P(ab)] indices are omitted. Consequently, in projections onto IP/EA doubly excited determinants $|\Phi^b_{ji}\rangle$, $|\Phi^{ba}_{j}\rangle$, indices belonging to the same particle or hole spaces are treated as non-equivalent.

3. **Equivalent indices in loop pairs:** Indices equivalent under the ring approximation are only considered as loop pairs, not individually. When one vertex corresponds to a two-electron integral, each such pair contributes a factor of $\frac{1}{2}$ (rather than $\frac{1}{4}$) owing to the direct approximation. For example, the following diagram



represents the drCCD correlation energy and is interpreted as $\frac{1}{2} \sum_{ijab} \langle ij|ab \rangle t_{ij}^{ab}$.

4. **Non-antisymmetrized two-electron integrals:** In the direct ring approximation, two-electron diagrams depict the non-antisymmetrized integrals $\langle pq|rs\rangle$ rather than $\langle pq||rs\rangle$. Consequently, the following two diagrams are not related via anti-symmetry



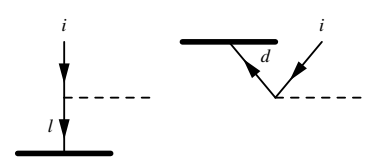
Similar to the second rule, two-body vertices may be mirrored (corresponding to the exchange of electrons 1 and 2), but the individual vertex lines cannot be exchanged independently.

5. Additional factors in density matrix diagrams: For diagrams contributing to the density matrices, special care must be taken for the *ovvo* (iabj) block of the two-body reduced density matrix Γ_{pars} .



Formally, the energy contribution is multiplied by a factor of 4 for each of the combinations iabj, aijb, aibj, and iajb, resulting in $4 \cdot \frac{1}{2} \sum_{iabj} \Gamma_{iabj} \langle ia|bj \rangle$. However, within the ring approximation, the aibj and iajb blocks are absent, which introduces an additional factor of $\frac{1}{2}$ in the contributions from $\Gamma_{iabj} \langle ia|bj \rangle$.

6. **Sign conventions for left and right EOM operators:** When the right EOM operator acts on the left $(\hat{R}_1^{\text{EA}\dagger}, \hat{R}_2^{\text{EA}\dagger})$ or the left EOM operator acts on the right $(\hat{L}_1^{\text{EA}\dagger}, \hat{L}_2^{\text{EA}\dagger})$, an additional factor of -1 must be included. This arises from the second term of the commutator. It is applied in addition to the standard sign factor $(-1)^K$, where K = l + h is the sum of the number of loops (l) and internal holes (h). For example, in the following diagrams:

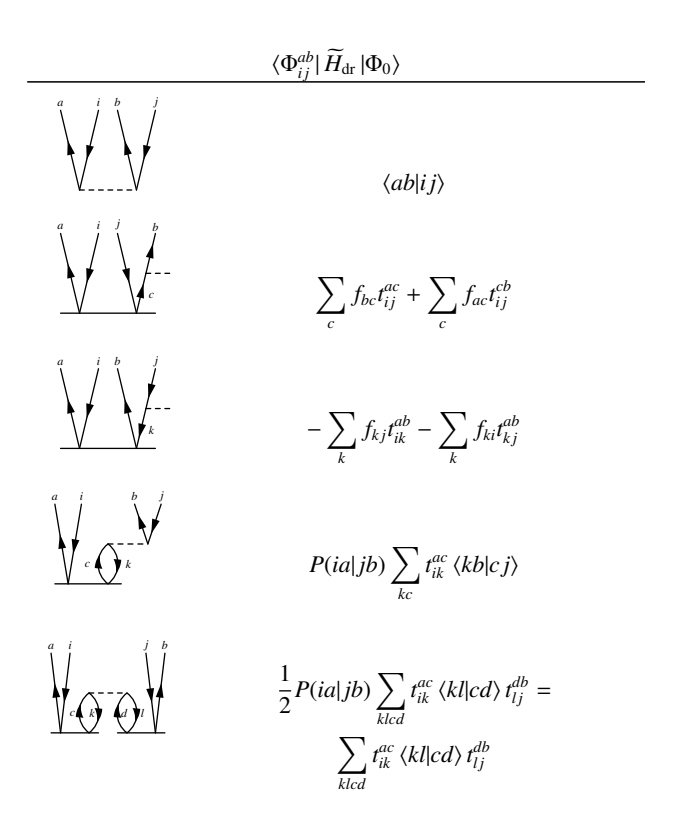


the overall sign in both cases is -1. In the first diagram, there is one internal hole and no loop (K=0+1), while in the second, there are neither loops nor internal holes (K=0), but the $\hat{R}_1^{\mathrm{EA}\dagger}$ operator acts on the left, introducing the additional negative sign.

Appendix B: drCCD working equations

The drCCD amplitude equations and the corresponding λ -amplitude equations are presented here in a diagrammatic and algebraic form.

1. drCCD amplitude equations



$$\langle \Phi_0 | \left(1+\hat{\Lambda}_2
ight) rac{\partial \widetilde{H}_{
m dr}}{\partial t_{ij}^{ab}} |\Phi_0
angle$$



$$\sum_{c} f_{cb} \lambda_{ac}^{ij} + \sum_{c} f_{ca} \lambda_{cb}^{ij}$$



$$-\sum_{k}f_{jk}\lambda_{ab}^{ik}-\sum_{k}f_{ik}\lambda_{ab}^{kj}$$

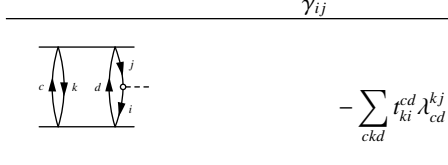


$$P(ia|jb) \sum_{kc} \lambda_{ac}^{ik} \langle cj|kb \rangle$$



$$P(ia|jb) \sum_{klcd} \lambda_{ac}^{ik} t_{kl}^{cd} \langle lj|db \rangle$$

3. One-electron density matrices

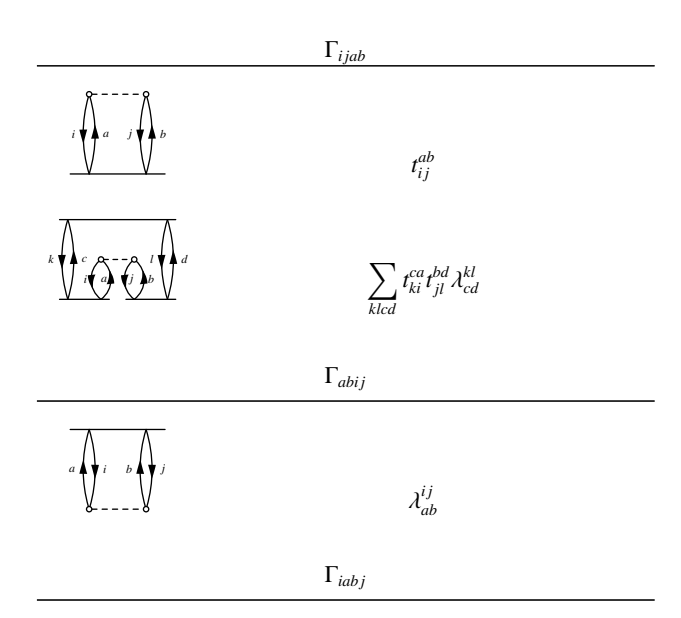






$$\sum_{ckl} t_{kl}^{cb} \lambda_{ca}^{kl}$$

4. Two-electron matrices





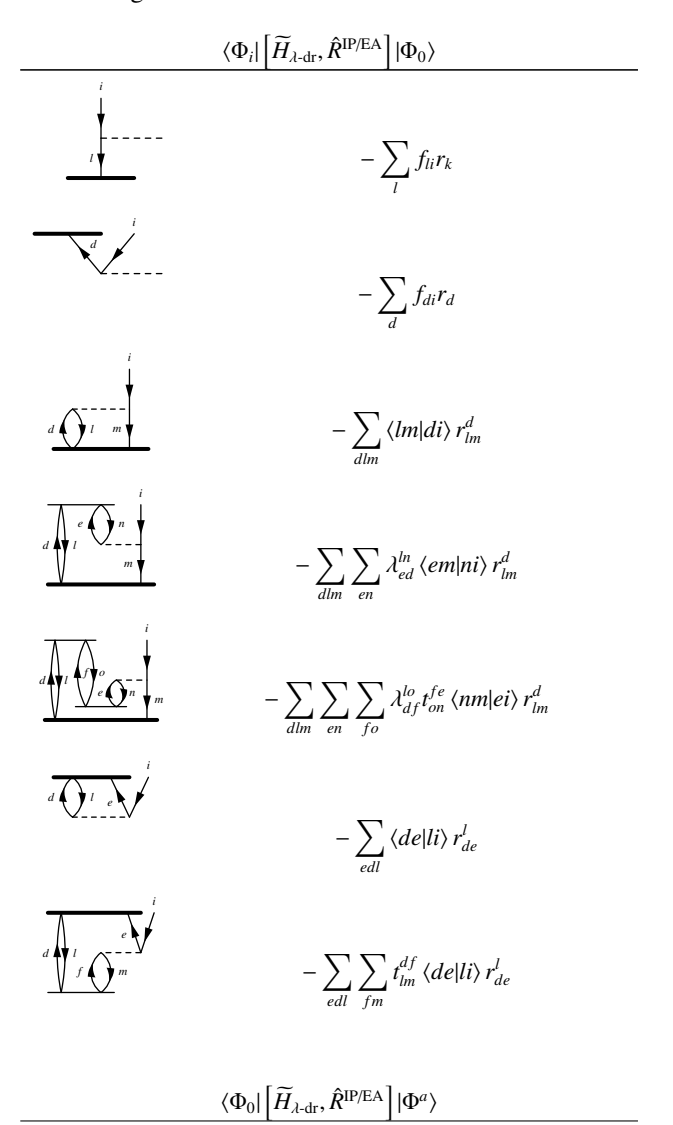
Appendix C: EA/IP-EOM-λ-drCCD working equations

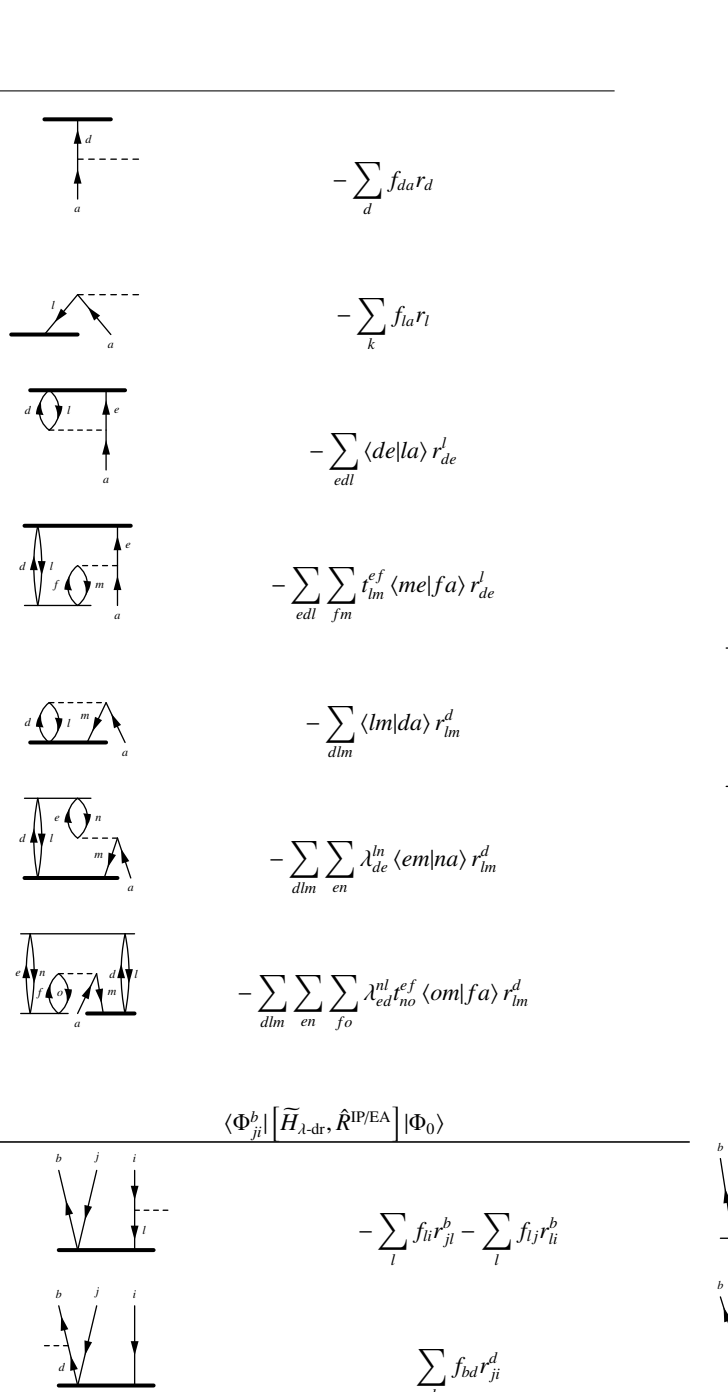
1. Right-EOM eigenvalue working equations

The right eigenvalue problem is divided into the singles IP and EA blocks, and the doubles IP and EA blocks, as follows:

$$\begin{split} r_{i}\epsilon^{\mathrm{IP/EA}} &= \langle \Phi_{i} | \left[\widetilde{H}_{\lambda\text{-dr}}, \hat{R}^{\mathrm{IP/EA}} \right] | \Phi_{0} \rangle \\ r_{a}\epsilon^{\mathrm{IP/EA}} &= \langle \Phi_{0} | \left[\widetilde{H}_{\lambda\text{-dr}}, \hat{R}^{\mathrm{IP/EA}} \right] | \Phi^{a} \rangle \\ r_{ji}^{b}\epsilon^{\mathrm{IP/EA}} &= \langle \Phi_{ji}^{b} | \left[\widetilde{H}_{\lambda\text{-dr}}, \hat{R}^{\mathrm{IP/EA}} \right] | \Phi_{0} \rangle \\ r_{ja}^{b}\epsilon^{\mathrm{IP/EA}} &= \langle \Phi_{0} | \left[\widetilde{H}_{\lambda\text{-dr}}, \hat{R}^{\mathrm{IP/EA}} \right] | \Phi_{j}^{ba} \rangle \end{split}$$
 (C1)

The evaluation of the required matrix elements is presented in the following tables.

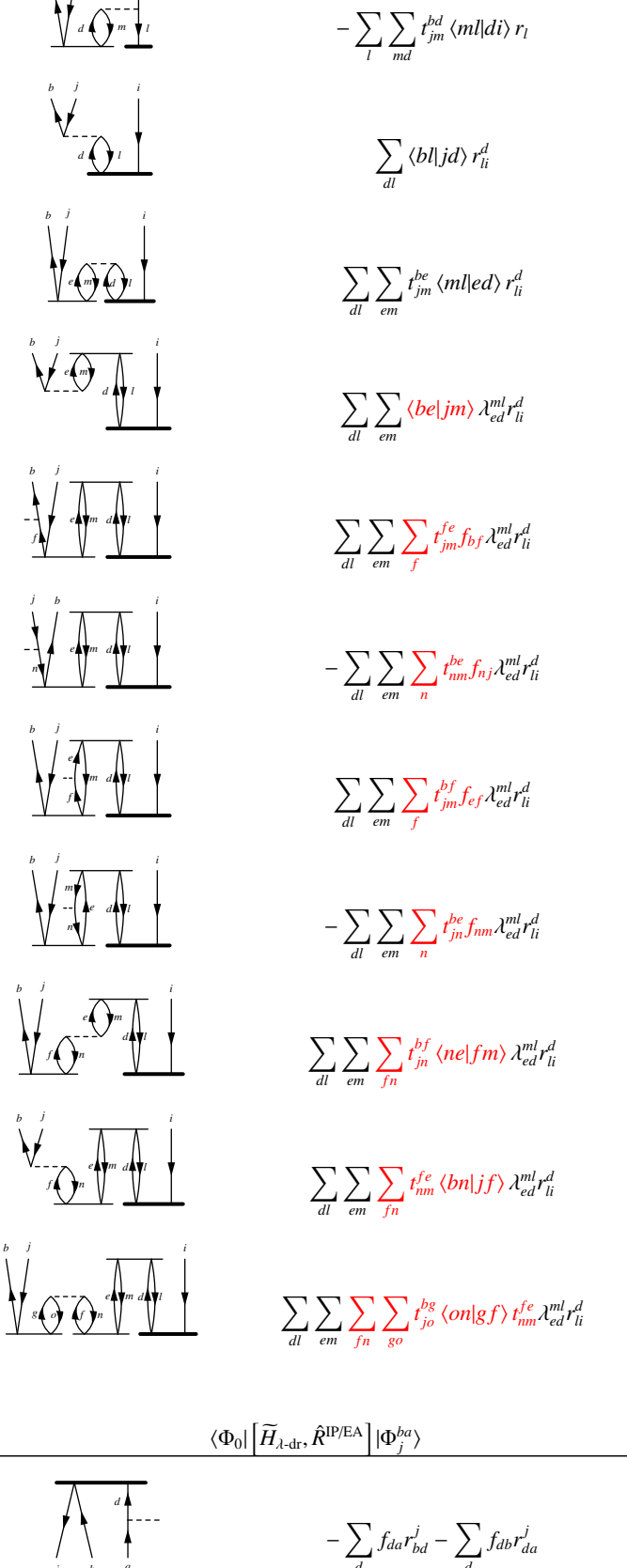


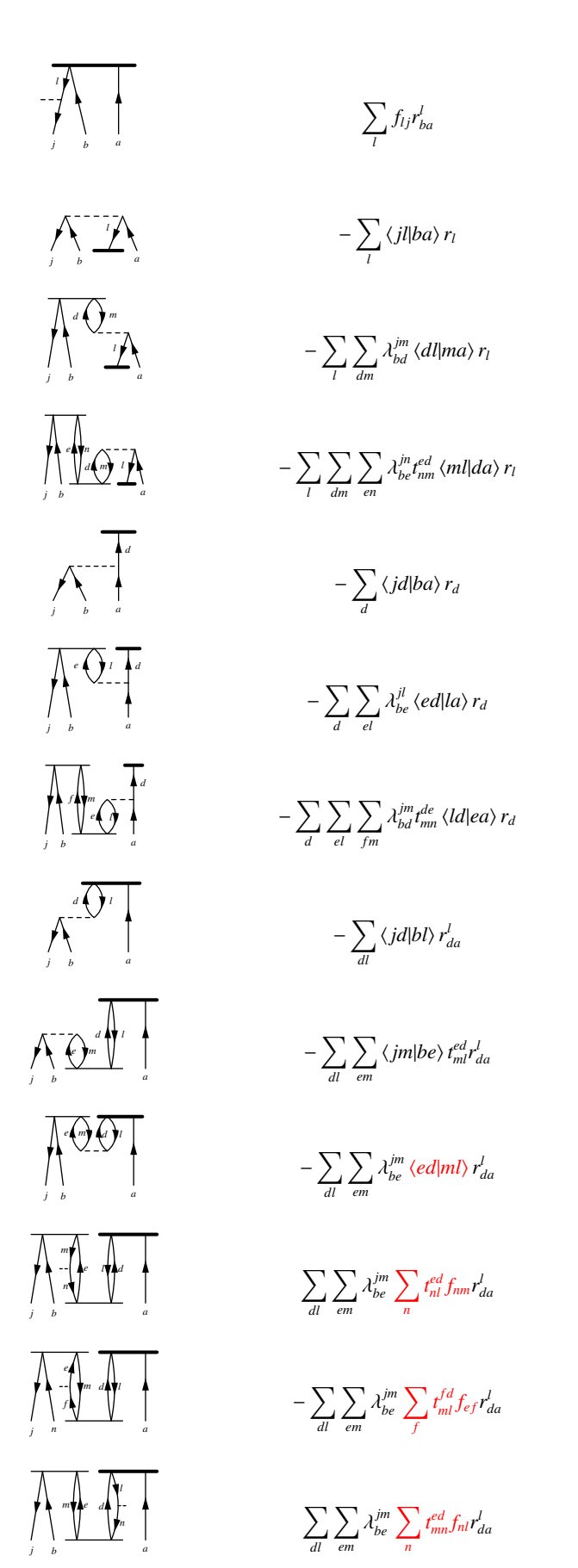


 $-\sum_i \langle bd|ji\rangle\,r_d$

 $-\sum_{d}\sum_{el}t_{jl}^{be}\left\langle ld|ei\right\rangle r_{d}$

 $-\sum_{l}\langle bl|ji\rangle\,r_{l}$





$$-\sum_{dl}\sum_{em}\lambda_{be}^{jm}\sum_{f}t_{ml}^{ed}f_{fd}r_{da}^{l}$$

$$-\sum_{dl}\sum_{em}\lambda_{be}^{jm}\sum_{fn}t_{ml}^{ed}\langle fm|ne\rangle r_{da}^{l}$$

$$-\sum_{dl}\sum_{em}\lambda_{be}^{jm}\sum_{fn}t_{ml}^{ed}\langle fm|ne\rangle r_{da}^{l}$$

$$-\sum_{dl}\sum_{em}\lambda_{be}^{jm}\sum_{fn}t_{mn}^{ef}\langle nd|fl\rangle r_{da}^{l}$$

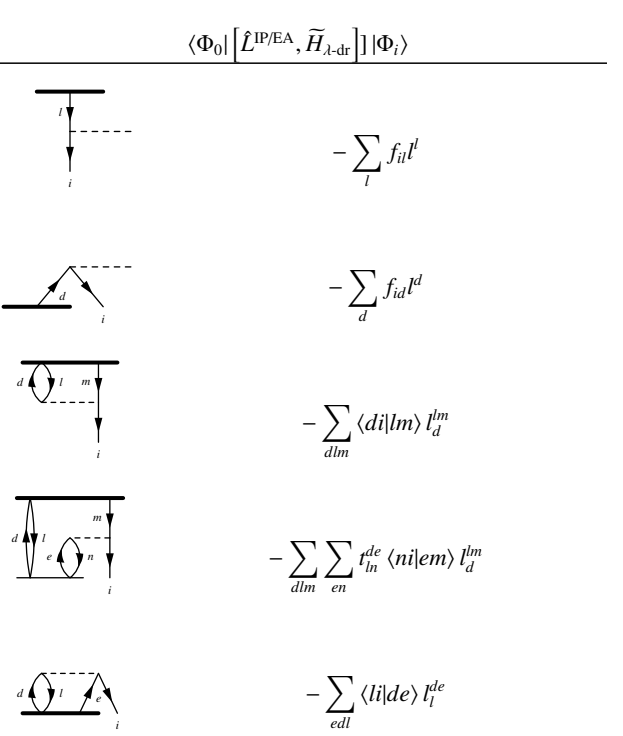
$$-\sum_{dl}\sum_{em}\lambda_{be}^{jm}\sum_{fn}\sum_{go}t_{mn}^{ef}\langle nd|fl\rangle r_{da}^{l}$$

2. Left-EOM eigenvalue working equations

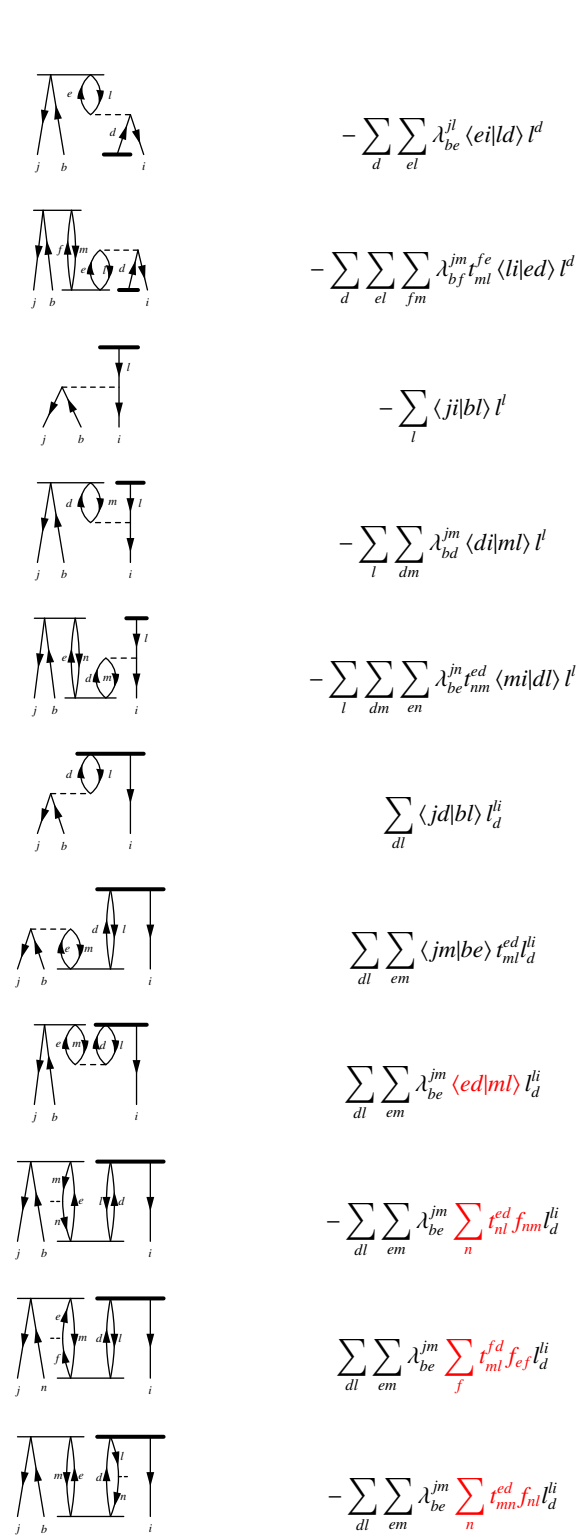
The left eigenvalue problem is divided into the singles IP and EA blocks, and the doubles IP and EA blocks, as follows:

$$\begin{split} \epsilon^{\text{IP/EA}} l^i &= \langle \Phi_0 | \left[\hat{L}^{\text{IP/EA}}, \widetilde{H}_{\lambda\text{-dr}} \right] | \Phi_i \rangle \\ \epsilon^{\text{IP/EA}} l^a &= \langle \Phi^a | \left[\hat{L}^{\text{IP/EA}}, \widetilde{H}_{\lambda\text{-dr}} \right] | \Phi_0 \rangle \\ \epsilon^{\text{IP/EA}} l_b^{ji} &= \langle \Phi_0 | \left[\hat{L}^{\text{IP/EA}}, \widetilde{H}_{\lambda\text{-dr}} \right] | \Phi_{ji}^b \rangle \\ \epsilon^{\text{IP/EA}} l_i^{ba} &= \langle \Phi_j^{ba} | \left[\hat{L}^{\text{IP/EA}}, \widetilde{H}_{\lambda\text{-dr}} \right] | \Phi_0 \rangle \end{split}$$
(C2)

The evaluation of the required matrix elements is presented in the following tables.

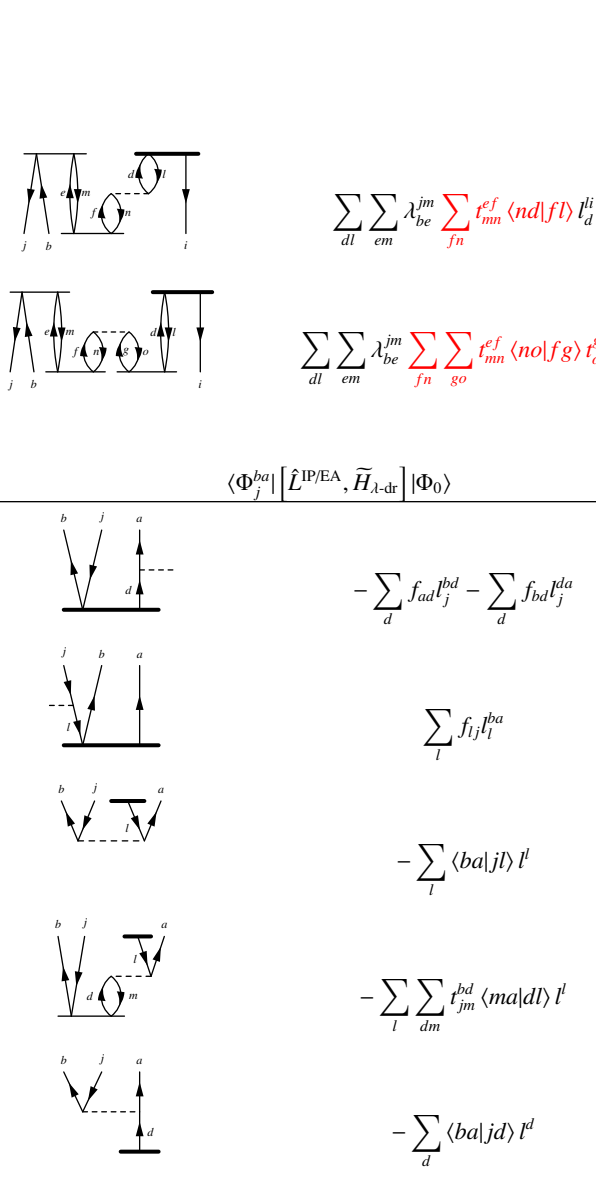


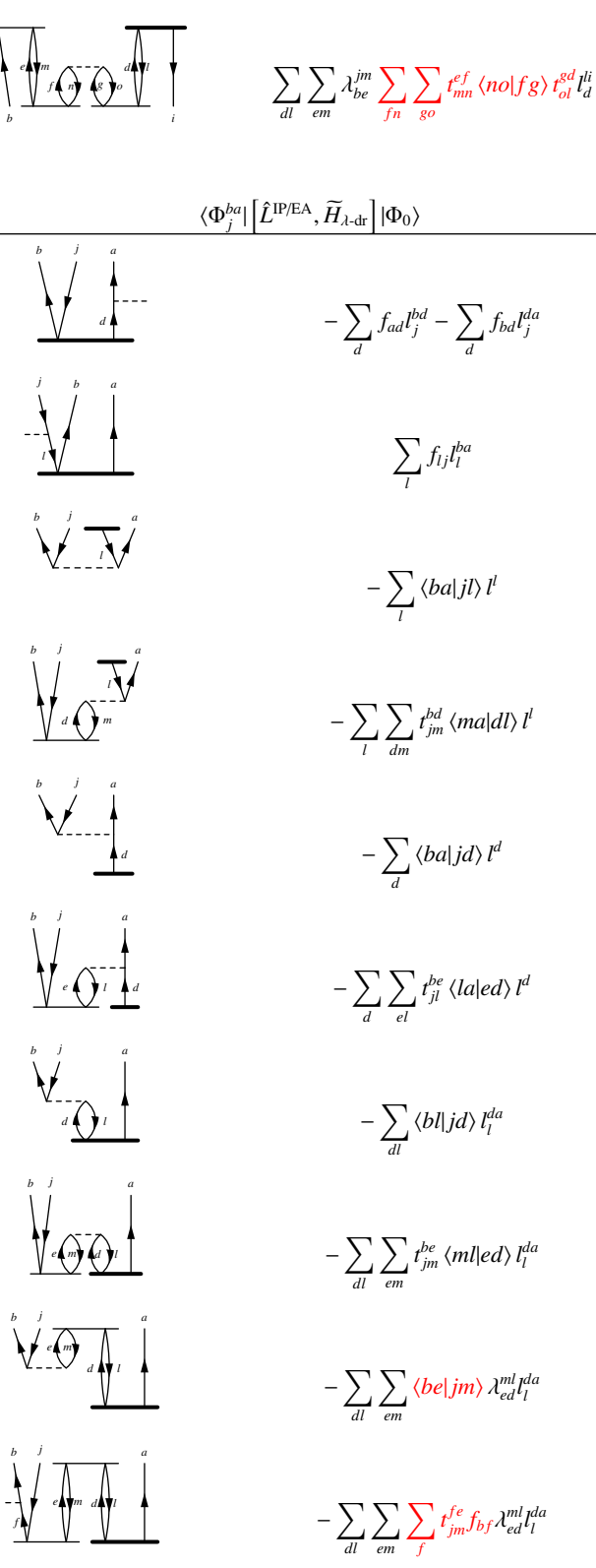
$d \bigwedge_{i}^{f} \underbrace{\bigcap_{e}^{m}}_{i}$	$-\sum_{edl}\sum_{fm}\lambda_{df}^{lm}\left\langle fi me ight angle l_{l}^{de}$	$\int_{J} \int_{b}^{c} \frac{1}{d\lambda} \int_{i}^{t}$
$ \int_{S} \int_{R} \int_{$	$-\sum_{edl}\sum_{fm}\sum_{gn}\lambda_{fd}^{ml}t_{mn}^{fg}\left\langle ni ge\right\rangle l_{l}^{de}$	$\int_{j}^{\infty} \int_{b}^{\infty} \frac{1}{d} \int_{i}^{\infty} \frac{1}{d} $
	$\langle \Phi^a \left[\hat{L}^{ ext{IP/EA}}, \widetilde{H}_{\lambda ext{-dr}} ight] \Phi_0 angle$	<u></u>
a 		
a a	$-\sum_d f_{ad} l^d$	
a a	$-\sum_l f_{ad}l^l$	
$d \underbrace{ \int I de }_{e}$	$-\sum_{edl} \left\langle la de ight angle l_l^{de}$	
$d \bigvee_{l} e \bigvee_{} a$	$-\sum_{\substack{edl \ en}} \sum_{\substack{en}} \lambda_{ed}^{ln} \langle ea ne \rangle l_l^{de}$	J 5 1
		$\int_{j}^{\infty} \int_{b}^{\infty} \int_{a}^{d} \int_{a}^{d} \int_{a}^{1} \int_{a}^{\infty} \int_{a$
V V M e	$-\sum_{edl}\sum_{fm}\sum_{gn}\lambda_{dg}^{ln}t_{nm}^{gf}\left\langle ma fe ight angle l_{l}^{de}$	
d 1 m	$-\sum_{dlm}raket{da lm}l_d^{lm}$	
m d		$\int_{j}^{\infty} \int_{b}^{-1} \int_{a}^{a} \int_{$
$d = \prod_{j=1}^{m} \prod_{i=1}^{m} n^{j}$	$-\sum_{dlm}\sum_{fn}t_{ln}^{df}\left\langle na fm ight angle l_{d}^{lm}$	e d m ddyl
	$\langle \Phi_0 \left[\hat{L}^{ ext{IP/EA}}, \widetilde{H}_{\lambda ext{-dr}} ight] \Phi^b_{jj} angle$	j n i
	$-\sum_l f_{il} l_b^{jl} - \sum_l f_{jl} l_b^{li}$	
	$\sum_d f_{db} l_d^{ji}$	$ \begin{array}{c c} & M & Ac \\ & M & A$
$\int_{j}^{-1} \int_{b}^{-1} \int_{i}^{d}$	$-\sum_d \braket{ji bd}{l^d}$	$\int_{j}^{m} \int_{b}^{e} \int_{n}^{d} \int_{1}^{d} \int_{1$

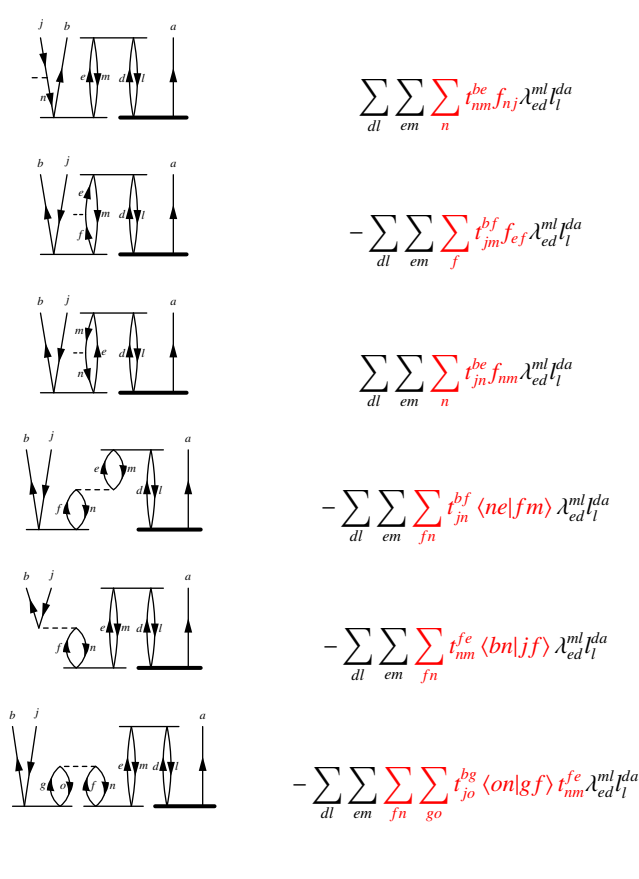


 $\sum_{dl} \sum_{em} \lambda_{be}^{jm} \sum_{f} t_{ml}^{ed} f_{fd} l_{d}^{li}$

 $\sum_{dl} \sum_{em} \lambda_{be}^{jm} \sum_{fn} t_{ml}^{ed} \langle fm|ne \rangle \, l_d^{li}$

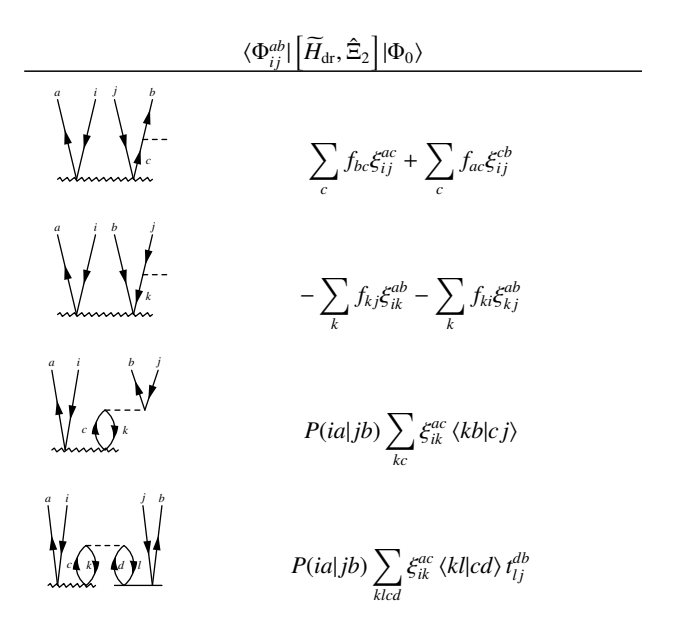






Contributions in red for the right- and left-EOM eigenvalue problem reproduce a projection of the drCCD Hamiltonian onto doubly excited determinants $\langle \Phi^{ab}_{ij} | \widetilde{H}_{dr} | \Phi_0 \rangle$. Since these projections are the CC amplitudes equations, they add up to zero and can be ignored in the implementation.

3. Ξ working equations

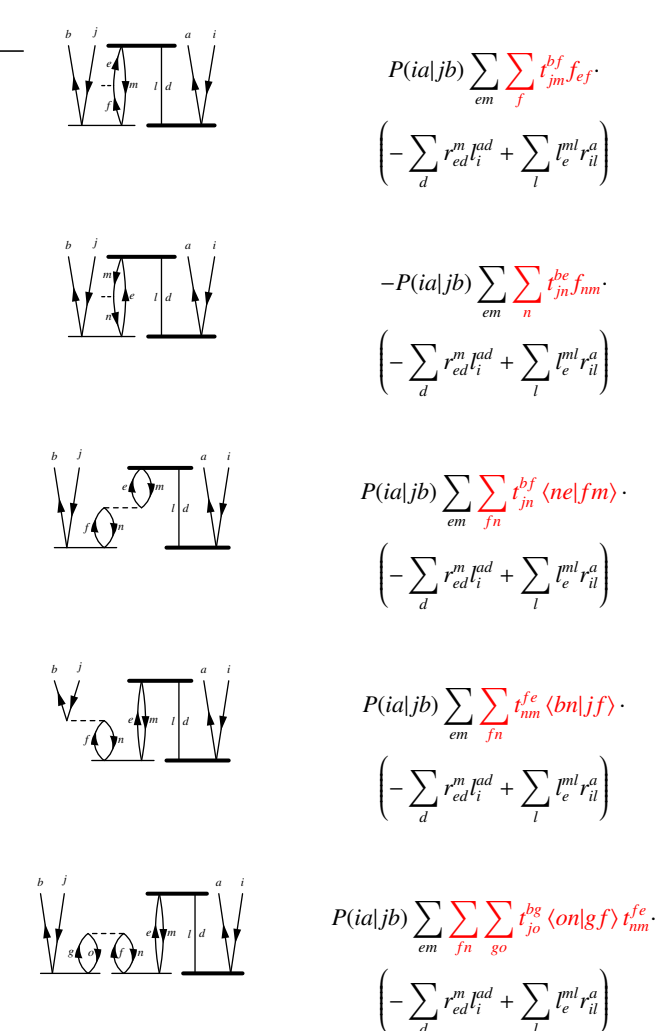


$\langle \Phi_0 igg[$	$\hat{L}^{ ext{IP/EA}}, \left[rac{\partial \widetilde{H}_{\lambda ext{-dr}}}{\partial \lambda_{ab}^{IJ}}, \hat{R}^{ ext{IP/EA}} ight] ight]_{+} \Phi_0 angle$
	$-P(ia jb)\sum_{ck}\langle ak ic\ranglel^cr^b_{jk}$
	$-P(ia jb)\sum_{ck}\sum_{dl}t_{il}^{ad}\left\langle lk dc\right\rangle l^{c}r_{jk}^{b}$
	$-P(ia jb)\sum_{ck}\langle ak ic\rangler_kl_j^{bc}$
$ \begin{array}{c} a i \\ \downarrow d \\ \downarrow d \\ \downarrow i \\ \downarrow d \end{array} $	$-P(ia jb)\sum_{ck}\sum_{dl}t_{il}^{ad}\left\langle lk dc\right\rangle r_{k}l_{j}^{bc}$
	$-P(ia jb)\sum_{kl}\langle ak il\ranglel^lr^b_{jk}$
$ \begin{array}{cccccccccccccccccccccccccccccccccccc$	$-P(ia jb)\sum_{kl}\sum_{dm}t_{im}^{ad}\left\langle mk dl ight angle l^{l}r_{jk}^{b}$
	$-P(ia jb)\sum_{cd}\langle ak ic angler_dl_j^{bc}$
$ \begin{array}{cccccccccccccccccccccccccccccccccccc$	$-P(ia jb)\sum_{cd}\sum_{el}t_{il}^{ae}\left\langle ld ec ight angle r_{d}l_{j}^{bc}$
	$P(ia jb)\sum_{em}\langle be jm\rangle$.
	$\left(-\sum_{d}r_{ed}^{m}l_{i}^{ad}+\sum_{l}l_{e}^{ml}r_{il}^{a} ight)$
	$P(ia jb) \sum_{em} \sum_{f} t_{jm}^{fe} f_{bf}.$

 $\left(-\sum_{i}r_{ed}^{m}l_{i}^{ad}+\sum_{i}l_{e}^{ml}r_{il}^{a}\right)$

 $-P(ia|jb)\sum_{em}\sum_{n}t_{nm}^{be}f_{nj}$

 $\left(-\sum_{d}r_{ed}^{m}l_{i}^{ad}+\sum_{l}l_{e}^{ml}r_{il}^{a}\right)$

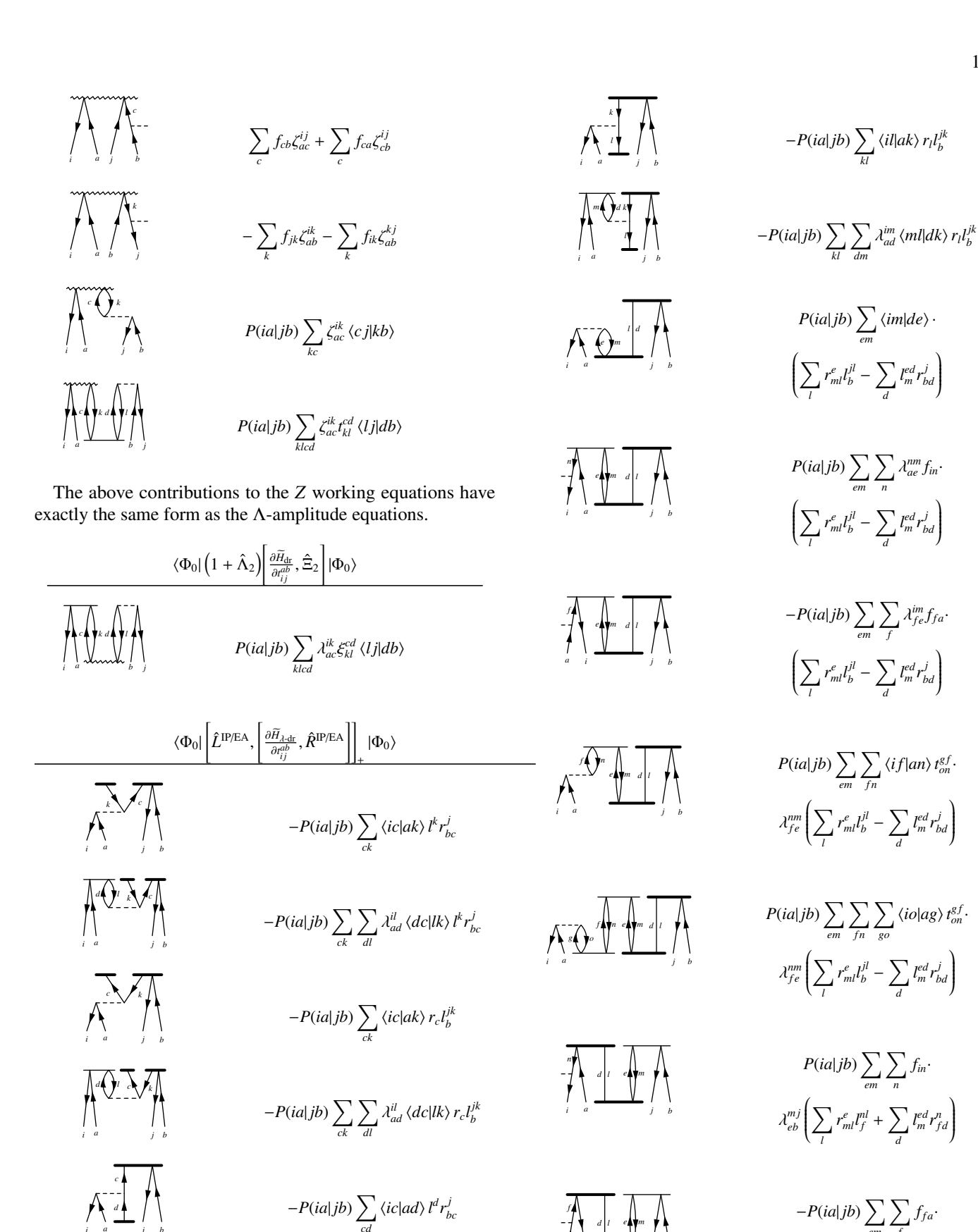


Contributions in red in the $\langle \Phi_0 | \left[\hat{L}^{IP/EA}, \left[\frac{\partial \widetilde{H}_{d\text{-}dr}}{\partial \lambda_{ab}^{IJ}}, \hat{R}^{IP/EA} \right] \right]_+ |\Phi_0 \rangle$ term reproduce a projection of the drCCD Hamiltonian onto doubly excited determinants $\langle \Phi_{ij}^{ab} | \widetilde{H}_{dr} | \Phi_0 \rangle$. Since these projections are the CC amplitudes equations, they add up to zero and can be ignored in the implementation. The complete $\langle \Phi_0 | \left[\hat{L}^{IP/EA}, \left[\frac{\partial \widetilde{H}_{d\text{-}dr}}{\partial \lambda_{ab}^{IJ}}, \hat{R}^{IP/EA} \right] \right]_+ |\Phi_0 \rangle$ contributions also need to be multiplied with the corresponding ± 1 prefactor.

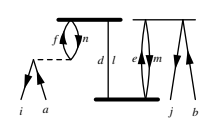
4. Z working equations

$$\langle \Phi_0 | \left(1+\hat{Z}_2
ight) rac{\partial \widetilde{H}_{
m dr}}{\partial t_{ij}^{ab}} |\Phi_0
angle$$

 $\lambda_{eb}^{mj} \left(\sum_{l} r_{ml}^{e} l_f^{nl} + \sum_{d} l_m^{ed} r_{fd}^n \right)$

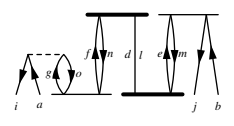


 $-P(ia|jb)\sum_{cd}\sum_{cl}\lambda_{ae}^{il}\langle ec|ld\rangle l^d r_{bc}^j$



$$P(ia|jb) \sum_{em} \sum_{fn} \langle if|an \rangle \cdot$$

$$\lambda_{eb}^{mj} \left(\sum_{l} r_{ml}^{e} l_{f}^{nl} + \sum_{d} l_{m}^{ed} r_{fd}^{n} \right)$$



$$P(ia|jb) \sum_{em} \sum_{fn} \sum_{go} \langle io|ag \rangle t_{on}^{gf}$$

$$\lambda_{eb}^{mj} \left(\sum_{l} r_{ml}^{e} l_{f}^{nl} + \sum_{d} l_{m}^{ed} r_{fd}^{n} \right)$$

The complete $\langle \Phi_0 | \left[\hat{L}^{IP/EA}, \left[\frac{\partial \widetilde{H}_{\lambda\text{-dr}}}{\partial l_{ij}^{ab}}, \hat{R}^{IP/EA} \right] \right]_+ |\Phi_0 \rangle$ contributions need to multiplied by the corresponding ± 1 prefactor.

5. One-electron density matrices

Contribution from $\langle \Phi_0 | \left[\hat{L}^{\text{IP/EA}}, \left[\widetilde{H}_{\lambda\text{-dr}}, \hat{R}^{\text{IP/EA}} \right] \right]_+ |\Phi_0 \rangle$



$$-r_i l$$



$$-\sum_{ck}r_{ki}^cl_c^{kj}+\sum_{ck}r_{ik}^cl_c^{jk}$$



$$\sum_{c,d} l_i^{dc} r_{dc}^j$$



$$-\sum_{em}\sum_{fn}\sum_{g}\lambda_{eg}^{mj}t_{in}^{gf}\cdot$$

$$\left(\sum_{l}l_{f}^{nl}r_{ml}^{e}-\sum_{d}r_{fd}^{n}l_{m}^{ed}\right)$$



$$-\sum_{em}\sum_{fn}\sum_{g}\lambda_{ef}^{mn}t_{ni}^{fg}\cdot$$

$$\left(\sum_{l}l_{g}^{jl}r_{ml}^{e}-\sum_{d}r_{gd}^{j}l_{m}^{ed}\right)$$

 γ_{ab}



$$-r_a l^b$$

$$-\sum_{ck}r_{cb}^{k}l_{k}^{ca}+\sum_{ck}r_{bc}^{k}l_{k}^{ac}$$



$$\sum_{kl} l_a^{lk} r_{lk}^b$$



$$\sum_{em} \sum_{fn} \sum_{g} \lambda_{ea}^{mo} t_{on}^{bf} \cdot$$

$$\left(\sum_{l}l_{f}^{nl}r_{ml}^{e}-\sum_{d}r_{fd}^{n}l_{m}^{ed}\right)$$



$$\sum_{em} \sum_{fn} \sum_{g} \lambda_{ef}^{mn} t_{no}^{fb} \cdot$$

$$\left(\sum_{l}l_{a}^{ol}r_{ml}^{e}-\sum_{d}r_{ad}^{o}l_{m}^{ed}
ight)$$

 γ_{ai}



 $r_a l^i$

 γ_{ia}



 $r_i l^a$

Contributions from $\langle \Phi_0 | \left[\hat{L}^{\text{IP/EA}}, \left[\widetilde{H}_{\lambda\text{-dr}}, \hat{R}^{\text{IP/EA}} \right] \right]_+ |\Phi_0 \rangle$ need to be multiplied with the corresponding ± 1 prefactor.

Contribution from $\langle \Phi_0 | \left(1 + \hat{\Lambda}_2 \right) \left[\widetilde{H}_{dr}, \hat{\Xi}_2 \right] | \Phi_0 \rangle$

 $c \downarrow k \qquad d \downarrow j$



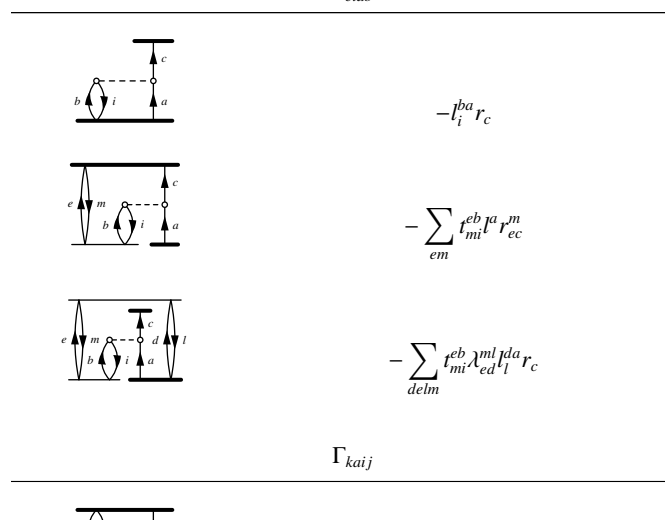
 γ_{ab}



$$\sum_{a^{kl}} \lambda^{kl}_{ca} \xi^{cb}_{kl}$$

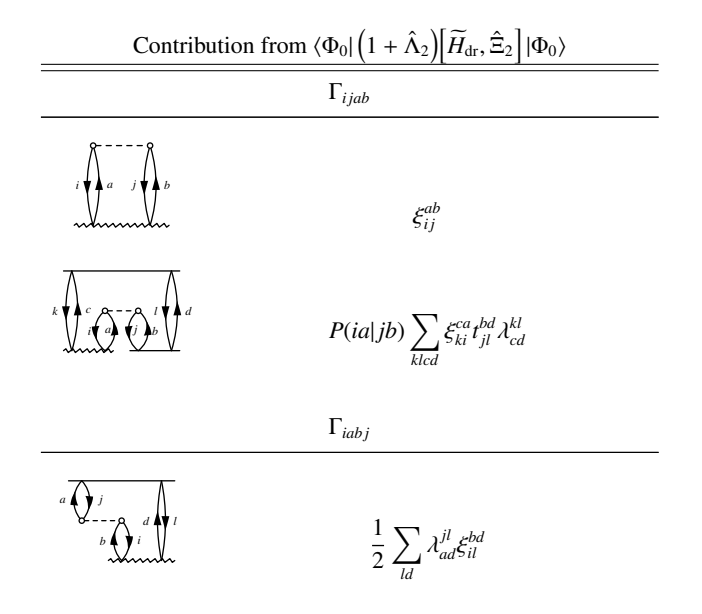
6. Two-electron density matrices

Contribution f	from $\langle \Phi_0 \left[\hat{L}^{ ext{IP/EA}}, \left[\widetilde{H}_{\lambda ext{-dr}}, \hat{R}^{ ext{IP/EA}} ight] ight]_+ \Phi_0 angle$	a	
	Γ_{abij}	b i 1	$-rac{1}{2}\sum_{dl}\lambda_{ad}^{jl}r_{li}^{d}l^{b}$
	$-P(ia jb)r_{ab}^{i}l^{j}$	$a \overbrace{\bigcup_{i} j}_{b} \underbrace{\int_{d} d \prod_{l} l}$	$-\frac{1}{2}\sum_{dl}\lambda_{ad}^{jl}l_{l}^{db}r_{i}$
	$-P(ia jb)l_a^{ij}r_b$	$b \underbrace{\int_{i}^{j} d}_{d} \underbrace{\int_{d}^{d} t}_{d}$	$-\frac{1}{2}\sum_{dl}t^{bd}_{il}r^l_{da}l^j$
	$P(ia jb) \sum_{ck} \lambda_{ca}^{ki} \left(\sum_{l} I_b^{jl} r_{kl}^c - \sum_{d} r_{bd}^j I_k^{cd} \right)$	$b \underbrace{\int_{i}^{d} \int_{d}^{d} \int_{d}^{d} I}_{d}$	$-\frac{1}{2}\sum_{dl}t_{il}^{bd}l_{d}^{lj}r_{a}$
	Γ_{ijab}	- A	15
$a \underbrace{0 \atop i \atop j}_{i} \underbrace{0 \atop b}_{b}$	$-P(ia jb)r_{ij}^{a}l^{b}$	$ \begin{array}{cccccccccccccccccccccccccccccccccccc$	$rac{1}{2}\sum_{cekm}t_{ik}^{bc}\lambda_{ce}^{km}. \ \left(\sum_{l}l_{a}^{jl}r_{ml}^{e}-\sum_{d}r_{ad}^{j}l_{m}^{ed} ight)$
$ \begin{array}{c c} c & k & b & d & d \\ \hline & & & & & & & & & & & & & & \\ c & & & & & & & & & & & & & & & \\ & & & & $	$-P(ia jb)\sum_{ck}\sum_{dl}t_{jl}^{bd}\lambda_{cd}^{kl}r_{ki}^{c}l^{a}$	$a = \begin{cases} j & \\ 0 & $	$rac{1}{2}\sum_{cekm}t_{ik}^{bc}\lambda_{ae}^{jm}.$
$a \underbrace{ \underbrace{ \underbrace{ i b }_{i} b }_{j} }_{j}$	$-P(ia jb)l_i^{ab}r_j$		$\left(\sum_{l}l_{c}^{kl}r_{ml}^{e}-\sum_{d}r_{cd}^{k}l_{m}^{ed} ight)$
$ \begin{array}{c c} c & k & b \\ \hline & b & j & j \end{array} $	$-P(ia jb)\sum_{ck}\sum_{dl}t_{jl}^{bd}\lambda_{cd}^{kl}l_{ca}^{k}r_{i}$		Γ_{ijka}
	$P(ia jb) \sum_{ck} t_{ki}^{ca} \left(\sum_{l} r_{jl}^{b} l_c^{kl} - \sum_{d} l_j^{bd} r_{cd}^{k} \right)$		$-r^a_{ji}I^k$ $-\sum_{em}t^{ea}_{mj}r_i l^{mk}_e$
	$P(ia jb) \sum_{cefkmn} t_{ki}^{ca} t_{jm}^{be} \lambda_{ef}^{mn} \cdot \ \left(\sum_{l} r_{nl}^{f} l_{c}^{kl} - \sum_{d} l_{n}^{fd} r_{cd}^{k} ight)$	$ \begin{array}{c c} c & m & k & d \\ d & j & i \end{array} $	$-\sum_{delm}t_{mj}^{ea}\lambda_{ed}^{ml}r_{ll}^{d}l^{k}$
	Γ_{iabj}		Γ_{kaij}
$a \overbrace{\bigcup_{i=1}^{j} j \atop b} \underbrace{1}_{i}$	$\frac{1}{2} \sum_{l} l_a^{jl} r_{il}^b - \frac{1}{2} \sum_{d} r_{ad}^j l_i^{bd}$	$ \begin{array}{cccccccccccccccccccccccccccccccccccc$	$-l_a^{ji}r_k \ -\sum \lambda_{ea}^{mj}l^ir_{mk}^e$





Contributions from $\langle \Phi_0 | \left[\hat{L}^{\text{IP/EA}}, \left[\widetilde{H}_{\lambda\text{-dr}}, \hat{R}^{\text{IP/EA}} \right] \right]_+ |\Phi_0 \rangle$ need to be multiplied with the corresponding ± 1 prefactor.



The one- and two-electron contributions need additional contributions from the $\langle \Phi_0 | \left(1+\hat{Z}_2\right) \frac{\partial H_{\rm dr}}{\partial t_0^{ab}} | \Phi_0 \rangle$ term. These are not repeated here, as they have exactly the same form as the ground-state drCCD contribution, where the $\hat{\Lambda}_2$ operator has been substituted by \hat{Z}_2 .

Appendix D: Connecting the G_0W_0 non-linear equation to the IP/EA-EOM- λ -drCCD parameters

In this appendix, a connection between the quantities derived from a conventional G_0W_0 implementation is related to the IP/EA-EOM- λ -drCCD quantities. This may aid in the implementation of the reduced density matrices within an existing G_0W_0 implementation.

1. Effective two-electron integrals

The effective integrals [see Eq. (6)] can be formally rewritten using the λ -drCCD amplitudes and the elements of the matrices X and \bar{X} (or alternatively the EOM-S-drCCD eigenvectors). The transformed fluctuation potential operator within the direct approximation is employed

$$e^{\hat{T}_2}\hat{V}_N e^{\hat{T}_2} + \left[\hat{\Lambda}_2, e^{\hat{T}_2}\hat{V}_N e^{\hat{T}_2}\right] \approx \widetilde{V}_{\lambda\text{-dr}}.$$
 (D1)

The following cases can be distinguished

$$(ai|\mu) = \langle \Phi_{il}^{ad} | \widetilde{V}_{\lambda-dr} | \Phi_0 \rangle x_{lu}^d,$$
 (D2a)

$$(ia|\mu) = \langle \Phi_I^d | \widetilde{V}_{\lambda - dr} | \Phi_i^a \rangle x_{I,u}^d, \tag{D2b}$$

$$(ab|\mu) = \langle \Phi_l^{da} | \widetilde{V}_{\lambda \text{-dr}} | \Phi^b \rangle x_{lu}^d, \tag{D2c}$$

$$(ij|\mu) = \langle \Phi_{li}^d | \widetilde{V}_{\lambda-dr} | \Phi_i \rangle x_{l,\mu}^d,$$
 (D2d)

$$(\mu|ai) = \bar{x}_{l,u}^{d*} \langle \Phi_0 | \widetilde{V}_{\lambda-dr} | \Phi_{il}^{ad} \rangle, \qquad (D2e)$$

$$(\mu|ia) = \bar{x}_{l,\mu}^{d*} \langle \Phi_i^a | \widetilde{V}_{\lambda\text{-dr}} | \Phi_l^d \rangle, \qquad (D2f)$$

$$(\mu|ab) = \bar{x}_{l,\mu}^{d*} \langle \Phi^b | \widetilde{V}_{\lambda\text{-dr}} | \Phi_l^{da} \rangle, \qquad (D2g)$$

$$(\mu|ij) = \bar{x}_{l,u}^{d*} \langle \Phi_i | \widetilde{V}_{\lambda-dr} | \Phi_{li}^d \rangle.$$
 (D2h)

The corresponding contributions can be assigned to diagrams presented in Appendix C.

2. The diagonal approximation

Within the diagonal approximation, as presented in Eq. (51), the right eigenvalue singles blocks take the form

$$r_{i}\epsilon_{i}^{G_{0}W_{0}} = -r_{i}\epsilon_{i}^{HF} + \sum_{dlm} \langle \Phi_{i} | \widetilde{V}_{\lambda - dr} | \Phi_{lm}^{d} \rangle r_{lm}^{d} - \sum_{e'l} \langle \Phi_{il}^{ed} | \widetilde{V}_{\lambda - dr} | \Phi_{0} \rangle r_{de}^{l}$$
(D3)

for the IP solutions and

$$r_{a}\epsilon_{a}^{G_{0}W_{0}} = -r_{a}\epsilon_{a}^{HF} + \sum_{dlm} \langle \Phi_{0} | \widetilde{V}_{\lambda\text{-dr}} | \Phi_{lm}^{da} \rangle r_{lm}^{d} - \sum_{edl} \langle \Phi_{l}^{de} | \widetilde{V}_{\lambda\text{-dr}} | \Phi^{a} \rangle r_{de}^{l}$$
(D4)

for the EA solutions. Dividing both equations by r_i or r_a results in

$$\begin{split} \epsilon_{i}^{G_{0}W_{0}} &= \epsilon_{i}^{\mathrm{HF}} - \sum_{dlm} \langle \Phi_{i} | \widetilde{V}_{\lambda\text{-dr}} | \Phi_{lm}^{d} \rangle r_{lm}^{d} / r_{i} \\ &+ \sum_{edl} \langle \Phi_{il}^{ed} | \widetilde{V}_{\lambda\text{-dr}} | \Phi_{0} \rangle r_{de}^{l} / r_{i} \end{split} \tag{D5}$$

for the IP solutions and

$$\begin{split} \epsilon_{a}^{G_{0}W_{0}} &= \epsilon_{a}^{\mathrm{HF}} - \sum_{dlm} \langle \Phi_{0} | \widetilde{V}_{\lambda\text{-dr}} | \Phi_{lm}^{da} \rangle \, r_{lm}^{d} / r_{a} \\ &+ \sum_{ell} \langle \Phi_{l}^{de} | \widetilde{V}_{\lambda\text{-dr}} | \Phi^{a} \rangle \, r_{de}^{l} / r_{a} \end{split} \tag{D6}$$

for the EA solutions.

Similar manipulations can be performed for the left eigenvalue problem within the diagonal approximation. The singles take the form

$$\begin{split} \epsilon_{i}^{G_{0}W_{0}}l^{i} &= -\epsilon_{i}^{\mathrm{HF}}l^{i} \\ &+ \sum_{dlm} \langle \Phi_{lm}^{d} | \widetilde{V}_{\lambda\text{-dr}} | \Phi_{i} \rangle \, l_{d}^{lm} \\ &- \sum_{ll} \langle \Phi_{0} | \widetilde{V}_{\lambda\text{-dr}} | \Phi_{il}^{ed} \rangle \, l_{l}^{de} \end{split} \tag{D7}$$

for the IP solutions and

$$\begin{split} \epsilon_{a}^{G_{0}W_{0}}l^{a} &= -\epsilon_{a}^{\mathrm{HF}}l^{a} \\ &+ \sum_{dlm} \langle \Phi_{lm}^{da} | \widetilde{V}_{\lambda\text{-dr}} | \Phi_{0} \rangle \, l_{d}^{lm} \\ &- \sum_{edl} \langle \Phi^{a} | \widetilde{V}_{\lambda\text{-dr}} | \Phi_{l}^{de} \rangle \, l_{l}^{de} \end{split} \tag{D8}$$

for the EA solutions. Dividing both sides by $l^{i/a}$ results in

$$\begin{split} \epsilon_{i}^{G_{0}W_{0}} &= \epsilon_{i}^{\text{HF}} \\ &- \sum_{dlm} \langle \Phi_{lm}^{d} | \widetilde{V}_{\lambda\text{-dr}} | \Phi_{i} \rangle \, l_{d}^{lm} / l^{i} \\ &+ \sum_{ll} \langle \Phi_{0} | \widetilde{V}_{\lambda\text{-dr}} | \Phi_{il}^{ed} \rangle \, l_{l}^{de} / l^{i} \end{split} \tag{D9}$$

for the electron-detachment energies and

$$\begin{split} \epsilon_{a}^{G_{0}W_{0}} &= \epsilon_{a}^{\mathrm{HF}} \\ &- \sum_{dlm} \langle \Phi_{lm}^{da} | \widetilde{V}_{\lambda\text{-dr}} | \Phi_{0} \rangle \, l_{d}^{lm} / l^{a} \\ &+ \sum_{l} \langle \Phi^{a} | \widetilde{V}_{\lambda\text{-dr}} | \Phi_{l}^{de} \rangle \, l_{l}^{de} / l^{a}. \end{split} \tag{D10}$$

for the electron-attached energies.

Equations (D5), (D6), (D9) and (D10) yield two important observations. First, these expressions eliminate the explicit dependence on the singles (1h and 1p configurations) amplitudes and allow the eigenvalue problem to be formulated entirely in terms of the doubles space (2h1p and 2p1h configurations). This transforms the original linear problem into a non-linear one involving only doubles contributions, as demonstrated in

Ref. 59. Second, a direct comparison with Eq. (8) reveals a one-to-one correspondence between the self-energy $\Sigma_{pp}(\omega=\epsilon_p^{G_0W_0})$ and the doubles contributions.

By exploiting Eq. (D2), the EOM amplitudes can be related to contributions to the self-energy. For the IP case, one finds

$$\begin{split} \frac{r_{lm}^{d}}{r_{i}} &= -\sum_{\mu} \frac{\sum_{d'l'} \langle \Phi_{l'm}^{d'} | \widetilde{V}_{\lambda\text{-dr}} | \Phi_{i} \rangle \, x_{l',\mu}^{d'} \bar{x}_{l,\mu}^{d*}}{\epsilon_{i}^{G_{0}W_{0}} - \epsilon_{m}^{\text{HF}} + \Omega_{\mu}} \\ &= -\sum_{\mu} \frac{(im|\mu) \bar{x}_{l,\mu}^{d*}}{\epsilon_{i}^{G_{0}W_{0}} - \epsilon_{m}^{\text{HF}} + \Omega_{\mu}}, \end{split} \tag{D11a}$$

$$\begin{split} \frac{r_{de}^{I}}{r_{i}} &= + \sum_{\mu} \frac{x_{l,\mu}^{d} \sum_{d'l'} \bar{x}_{l',\mu}^{d'*} \langle \Phi_{0} | \widetilde{V}_{\lambda\text{-dr}} | \Phi_{il'}^{ed'} \rangle}{\epsilon_{i}^{G_{0}W_{0}} - \epsilon_{e}^{\text{HF}} + \Omega_{\mu}} \\ &= + \sum_{\mu} \frac{x_{l,\mu}^{d} (\mu | ei)}{\epsilon_{i}^{G_{0}W_{0}} - \epsilon_{e}^{\text{HF}} + \Omega_{\mu}}. \end{split} \tag{D11b}$$

For the EA case, the corresponding expressions are

$$\begin{split} \frac{r_{lm}^{d}}{r_{a}} &= -\sum_{\mu} \frac{\sum_{d'l'} \langle \Phi_{ml'}^{ad'} | \widetilde{V}_{\lambda\text{-dr}} | \Phi_{0} \rangle \, x_{l',\mu}^{d'} \overline{x}_{l,\mu}^{d*}}{\epsilon_{a}^{G_{0}W_{0}} - \epsilon_{m}^{\text{HF}} + \Omega_{\mu}} \\ &= -\sum_{\mu} \frac{(am|\mu) \bar{x}_{l,\mu}^{d*}}{\epsilon_{a}^{G_{0}W_{0}} - \epsilon_{m}^{\text{HF}} + \Omega_{\mu}}, \end{split} \tag{D12a}$$

$$\begin{split} \frac{r_{de}^{J}}{r_{a}} &= + \sum_{\mu} \frac{x_{l,\mu}^{d} \sum_{d'l'} \overline{x}_{l',\mu}^{d'*} \langle \Phi^{a} | \widetilde{V}_{\lambda\text{-dr}} | \Phi_{l'}^{d'e} \rangle}{\epsilon_{a}^{G_{0}W_{0}} - \epsilon_{e}^{\text{HF}} + \Omega_{\mu}} \\ &= + \sum_{\mu} \frac{x_{l,\mu}^{d} (\mu | ea)}{\epsilon_{a}^{G_{0}W_{0}} - \epsilon_{e}^{\text{HF}} + \Omega_{\mu}}. \end{split} \tag{D12b}$$

Following a similar procedure to the right-EOM amplitudes, the relationship of the left-EOM amplitudes to the frequencydependent terms reads

$$\begin{split} \frac{l_{d}^{lm}}{l^{i}} &= -\sum_{\mu} \frac{x_{l,\mu}^{d} \sum_{d'l'} \bar{x}_{l',\mu}^{d'*} \langle \Phi_{i} | \widetilde{V}_{\lambda\text{-dr}} | \Phi_{l'm}^{d'} \rangle}{\epsilon_{i}^{G_{0}W_{0}} - \epsilon_{m}^{\text{HF}} + \Omega_{\mu}} \\ &= -\sum_{\mu} \frac{x_{l,\mu}^{d} (\mu | im)}{\epsilon_{i}^{G_{0}W_{0}} - \epsilon_{m}^{\text{HF}} + \Omega_{\mu}}, \end{split} \tag{D13a}$$

$$\begin{split} \frac{l_{l}^{de}}{l^{i}} &= + \sum_{\mu} \frac{\sum_{d'l'} \langle \Phi_{il'}^{ed'} | \widetilde{V}_{\lambda\text{-dr}} | \Phi_{0} \rangle \, x_{l',\mu}^{d'} \bar{x}_{l,\mu}^{d*}}{\epsilon_{i}^{G_{0}W_{0}} - \epsilon_{e}^{\text{HF}} + \Omega_{\mu}} \\ &= + \sum_{\mu} \frac{(ei|\mu) \bar{x}_{l,\mu}^{d*}}{\epsilon_{i}^{G_{0}W_{0}} - \epsilon_{e}^{\text{HF}} + \Omega_{\mu}}. \end{split} \tag{D13b}$$

for the IP case, and

$$\begin{split} \frac{l_{d}^{lm}}{l^{a}} &= -\sum_{\mu} \frac{x_{l,\mu}^{d} \sum_{d'l'} \bar{x}_{l',\mu}^{d'*} \langle \Phi_{0} | \widetilde{V}_{\lambda\text{-dr}} | \Phi_{ml'}^{ad'} \rangle}{\epsilon_{a}^{G_{0}W_{0}} - \epsilon_{m}^{\text{HF}} + \Omega_{\mu}} \\ &= -\sum_{\mu} \frac{x_{l,\mu}^{d} (\mu | am)}{\epsilon_{a}^{G_{0}W_{0}} - \epsilon_{m}^{\text{HF}} + \Omega_{\mu}}, \\ \frac{l_{l}^{de}}{l^{a}} &= +\sum_{\mu} \frac{\sum_{d'l'} \langle \Phi_{l'}^{d'e} | \widetilde{V}_{\lambda\text{-dr}} | \Phi^{a} \rangle x_{l',\mu}^{d'} \bar{x}_{l,\mu}^{d*}}{\epsilon_{a}^{G_{0}W_{0}} - \epsilon_{e}^{\text{HF}} + \Omega_{\mu}} \\ &= +\sum_{\mu} \frac{(ea|\mu) \bar{x}_{l,\mu}^{d*}}{\epsilon_{a}^{G_{0}W_{0}} - \epsilon_{e}^{\text{HF}} + \Omega_{\mu}}. \end{split} \tag{D14b}$$

for the EA case.

REFERENCES

- ¹T. Baer and R. P. Tuckett, "Advances in threshold photoelectron spectroscopy (tpes) and threshold photoelectron photoion coincidence (tpepico)," Phys. Chem. Chem. Phys. **19**, 9698–9723 (2017).
- ²N. C. Handy and I. Schaefer, Henry F., "On the evaluation of analytic energy derivatives for correlated wave functions," J. Chem. Phys. **81**, 5031–5033 (1984)
- ³H. F. Schaefer and Y. Yamaguchi, "A new dimension to quantum chemistry: Theoretical methods for the analytic evaluation of first, second, and third derivatives of the molecular electronic energy with respect to nuclear coordinates," J. Mol. Struct. (THEOCHEM) 135, 369–390 (1986).
- ⁴P. Pulay, "Analytical derivatives, forces, force constants, molecular geometries, and related response properties in electronic structure theory," WIREs Comput. Mol. Sci. 4, 169–181 (2014).
- ⁵J. W. Park, R. Al-Saadon, M. K. MacLeod, T. Shiozaki, and B. Vlaisavljevich, "Multireference electron correlation methods: Journeys along potential energy surfaces," Chem. Rev. **120**, 5878–5909 (2020).
- ⁶H. Lischka, D. Nachtigallová, A. J. A. Aquino, P. G. Szalay, F. Plasser, F. B. C. Machado, and M. Barbatti, "Multireference approaches for excited states of molecules," Chem. Rev. 118, 7293–7361 (2018).
- ⁷J. Stålring, A. Bernhardsson, and R. Lindh, "Analytical gradients of a state average mcscf state and a state average diagnostic," Mol. Phys. 99, 103–114 (2001).
- ⁸P. Celani and H.-J. Werner, "Analytical energy gradients for internally contracted second-order multireference perturbation theory," J. Chem. Phys. 119, 5044–5057 (2003).
- ⁹P. G. Szalay, T. Müller, G. Gidofalvi, H. Lischka, and R. Shepard, "Multi-configuration self-consistent field and multireference configuration interaction methods and applications," Chem. Rev. 112, 108–181 (2012).
- ¹⁰T. Iino, T. Shiozaki, and T. Yanai, "Algorithm for analytic nuclear energy gradients of state averaged dmrg-cassef theory with newly derived coupled-perturbed equations," J. Chem. Phys. 158, 054107 (2023).
- ¹¹D. J. Rowe, "Equations-of-Motion Method and the Extended Shell Model," Rev. Mod. Phys. 40, 153–166 (1968).
- ¹²K. Sneskov and O. Christiansen, "Excited state coupled cluster methods," WIREs Comput. Mol. Sci. 2, 566–584 (2012).
- ¹³L. Hedin, "New method for calculating the one-particle Green's function with application to the electron-gas problem," Phys. Rev. 139, A796 (1965).
- ¹⁴F. Aryasetiawan and O. Gunnarsson, "The GW Method," Rep. Prog. Phys. 61, 237–312 (1998).
- ¹⁵L. Reining, "The GW approximation: Content, successes and limitations: The GW approximation," Wiley Interdiscip. Rev. Comput. Mol. Sci. 8, e1344 (2017).
- ¹⁶D. Golze, M. Dvorak, and P. Rinke, "The gw compendium: A practical guide to theoretical photoemission spectroscopy," Front. Chem. 7, 377 (2019).

- ¹⁷A. Marie, A. Ammar, and P.-F. Loos, "The GW approximation: A quantum chemistry perspective," in Advances in Quantum Chemistry, Novel Treatments of Strong Correlations, Vol. 90 (2024) pp. 157–184.
- ¹⁸G. Onida, L. Reining, and A. Rubio, "Electronic excitations: Density-functional versus many-body green's function approaches," Rev. Mod. Phys. 74, 601–659 (2002).
- ¹⁹R. M. Martin, L. Reining, and D. M. Ceperley, *Interacting Electrons: The-ory and Computational Approaches* (Cambridge University Press, 2016).
- ²⁰M. J. van Setten, F. Caruso, S. Sharifzadeh, X. Ren, M. Scheffler, F. Liu, J. Lischner, L. Lin, J. R. Deslippe, S. G. Louie, C. Yang, F. Weigend, J. B. Neaton, F. Evers, and P. Rinke, "GW 100: Benchmarking G₀W₀ for Molecular Systems," J. Chem. Theory Comput. 11, 5665–5687 (2015).
- ²¹F. Caruso, M. Dauth, M. J. van Setten, and P. Rinke, "Benchmark of gw approaches for the gw100 test set," J. Chem. Theory Comput. 12, 5076 (2016).
- ²²K. Krause and W. Klopper, "Implementation of the bethe-salpeter equation in the turbomole program," J. Comput. Chem. 38, 383–388 (2017).
- ²³ A. M. Lewis and T. C. Berkelbach, "Vertex corrections to the polarizability do not improve the gw approximation for the ionization potential of molecules," J. Chem. Theory Comput. 15, 2925 (2019).
- ²⁴F. Bruneval, N. Dattani, and M. J. van Setten, "The gw miracle in many-body perturbation theory for the ionization potential of molecules," Front. Chem. 9, 749779 (2021).
- ²⁵E. Monino and P.-F. Loos, "Connections and performances of green's function methods for charged and neutral excitations," J. Chem. Phys. 159, 034105 (2023).
- ²⁶A. Marie and P.-F. Loos, "Reference Energies for Valence Ionizations and Satellite Transitions," J. Chem. Theory Comput. 20, 4751–4777 (2024).
- ²⁷M. J. van Setten, R. Costa, F. Viñes, and F. Illas, "Assessing GW Approaches for Predicting Core Level Binding Energies," J. Chem. Theory Comput. 14, 877–883 (2018).
- ²⁸D. Golze, J. Wilhelm, M. J. van Setten, and P. Rinke, "Core-level binding energies from gw: An efficient full-frequency approach within a localized basis," J. Chem. Theory Comput. 14, 4856–4869 (2018).
- ²⁹D. Golze, L. Keller, and P. Rinke, "Accurate absolute and relative core-level binding energies from gw," J. Phys. Chem. Lett. 11, 1840–1847 (2020).
- ³⁰D. Mejia-Rodriguez, A. Kunitsa, E. Aprà, and N. Govind, "Scalable Molecular GW Calculations: Valence and Core Spectra," J. Chem. Theory Comput. 17, 7504–7517 (2021).
- ³¹ J. Li, Y. Jin, P. Rinke, W. Yang, and D. Golze, "Benchmark of gw methods for core-level binding energies," J. Chem. Theory Comput. 18, 7570–7585 (2022).
- ³²I. Mukatayev, F. Moevus, B. Sklénard, V. Olevano, and J. Li, "XPS Core-Level Chemical Shift by Ab Initio Many-Body Theory," J. Phys. Chem. A 127, 1642–1648 (2023).
- ³³R. L. Panadés-Barrueta and D. Golze, "Accelerating core-level gw calculations by combining the contour deformation approach with the analytic continuation of w," J. Chem. Theory Comput. 19, 5450–5464 (2023).
- ³⁴L. Gallandi, N. Marom, P. Rinke, and T. Körzdörfer, "Accurate Ionization Potentials and Electron Affinities of Acceptor Molecules II: Non-Empirically Tuned Long-Range Corrected Hybrid Functionals," J. Chem. Theory Comput. 12, 605–614 (2016).
- ³⁵R. M. Richard, M. S. Marshall, O. Dolgounitcheva, J. V. Ortiz, J.-L. Brédas, N. Marom, and C. D. Sherrill, "Accurate Ionization Potentials and Electron Affinities of Acceptor Molecules I. Reference Data at the CCSD(T) Complete Basis Set Limit," J. Chem. Theory Comput. 12, 595–604 (2016).
- ³⁶J. W. Knight, X. Wang, L. Gallandi, O. Dolgounitcheva, X. Ren, J. V. Ortiz, P. Rinke, T. Körzdörfer, and N. Marom, "Accurate Ionization Potentials and Electron Affinities of Acceptor Molecules III: A Benchmark of *GW* Methods," J. Chem. Theory Comput. 12, 615–626 (2016).
- ³⁷O. Dolgounitcheva, M. Díaz-Tinoco, V. G. Zakrzewski, R. M. Richard, N. Marom, C. D. Sherrill, and J. V. Ortiz, "Accurate Ionization Potentials and Electron Affinities of Acceptor Molecules IV: Electron-Propagator Methods," J. Chem. Theory Comput. 12, 627–637 (2016).
- ³⁸A. Marie, P. Romaniello, and P.-F. Loos, "Anomalous propagators and the particle-particle channel: Hedin's equations," Phys. Rev. B 110, 115155 (2024).
- ³⁹D. Neuhauser, E. Rabani, and R. Baer, "Expeditious stochastic calculation of random-phase approximation energies for thousands of electrons in three dimensions," J. Phys. Chem. Lett. 4, 1172–1176 (2013).

- ⁴⁰D. Neuhauser, Y. Gao, C. Arntsen, C. Karshenas, E. Rabani, and R. Baer, "Breaking the Theoretical Scaling Limit for Predicting Quasiparticle Energies: The Stochastic GW Approach," Phys. Rev. Lett. 113, 076402 (2014).
- ⁴¹M. Kaltak, J. Klimeš, and G. Kresse, "Low scaling algorithms for the random phase approximation: Imaginary time and laplace transformations," J. Chem. Theory Comput. 10, 2498–2507 (2014).
- ⁴²M. Govoni and G. Galli, "Large scale GW calculations," J. Chem. Theory Comput. 11, 2680–2696 (2015).
- ⁴³V. Vlček, E. Rabani, D. Neuhauser, and R. Baer, "Stochastic GW Calculations for Molecules," J. Chem. Theory Comput. 13, 4997–5003 (2017).
- ⁴⁴J. Wilhelm, D. Golze, L. Talirz, J. Hutter, and C. A. Pignedoli, "Toward gw calculations on thousands of atoms," J. Phys. Chem. Lett. 9, 306–312 (2018).
- ⁴⁵I. Duchemin and X. Blase, "Separable resolution-of-the-identity with allelectron gaussian bases: Application to cubic-scaling rpa," J. Chem. Phys. 150, 174120 (2019).
- ⁴⁶M. D. Ben, F. H. da Jornada, A. Canning, N. Wichmann, K. Raman, R. Sasanka, C. Yang, S. G. Louie, and J. Deslippe, "Large-scale GW calculations on pre-exascale HPC systems," Comp. Phys. Comm. 235, 187–195 (2019).
- ⁴⁷ A. Förster and L. Visscher, "Low-order scaling g0w0 by pair atomic density fitting," J. Chem. Theory Comput. 16, 7381–7399 (2020).
- ⁴⁸I. Duchemin and X. Blase, "Robust analytic-continuation approach to many-body GW calculations," J. Chem. Theory Comput. 16, 1742–1756 (2020).
- ⁴⁹M. Kaltak and G. Kresse, "Minimax isometry method: A compressive sensing approach for matsubara summation in many-body perturbation theory," Phys. Rev. B 101, 205145 (2020).
- ⁵⁰ A. Förster and L. Visscher, "Low-order scaling quasiparticle self-consistent gw for molecules," Front. Chem. 9, 736591 (2021).
- 51 L. Duchemin and X. Blase, "Cubic-scaling all-electron gw calculations with a separable density-fitting space–time approach," J. Chem. Theory Comput. 17, 2383–2393 (2021).
- ⁵²J. Wilhelm, P. Seewald, and D. Golze, "Low-Scaling GW with Benchmark Accuracy and Application to Phosphorene Nanosheets," J. Chem. Theory Comput. 17, 1662–1677 (2021).
- ⁵³A. Förster and L. Visscher, "Quasiparticle Self-Consistent GW-Bethe-Salpeter Equation Calculations for Large Chromophoric Systems," J. Chem. Theory Comput. 18, 6779–6793 (2022).
- ⁵⁴V. W.-z. Yu and M. Govoni, "GPU Acceleration of Large-Scale Full-Frequency GW Calculations," J. Chem. Theory Comput. 18, 4690–4707 (2022).
- ⁵⁵J. Tölle, N. Niemeyer, and J. Neugebauer, "Accelerating analytic-continuation gw calculations with a laplace transform and natural auxiliary functions," J. Chem. Theory Comput. 20, 2022–2032 (2024).
- ⁵⁶E. A. Vo, X. Wang, and T. C. Berkelbach, "Performance of periodic eomcommunication of communication of periodic eomcommunication of communication of
- ⁵⁷E. Moerman, A. Gallo, A. Irmler, T. Schäfer, F. Hummel, A. Grüneis, and M. Scheffler, "Finite-size effects in periodic eom-ccsd for ionization energies and electron affinities: Convergence rate and extrapolation to the thermodynamic limit," J. Chem. Theory Comput. 21, 1865–1878 (2025).
- ⁵⁸M. F. Lange and T. C. Berkelbach, "On the Relation between Equation-of-Motion Coupled-Cluster Theory and the *GW* Approximation," J. Chem. Theory. Comput. 14, 4224–4236 (2018).
- ⁵⁹R. Quintero-Monsebaiz, E. Monino, A. Marie, and P.-F. Loos, "Connections between many-body perturbation and coupled-cluster theories," J. Chem. Phys. 157, 231102 (2022).
- ⁶⁰J. Tölle and G. K.-L. Chan, "Exact relationships between the gw approximation and equation-of-motion coupled-cluster theories through the quasi-boson formalism," J. Chem. Phys. 158, 124123 (2023).
- ⁶¹J. Čížek, "On the Correlation Problem in Atomic and Molecular Systems. Calculation of Wavefunction Components in Ursell-Type Expansion Using Quantum-Field Theoretical Methods," J. Chem. Phys. 45, 4256–4266 (1966).
- ⁶²J. Paldus, J. Čížek, and I. Shavitt, "Correlation problems in atomic and molecular systems. iv. extended coupled-pair many-electron theory and its application to the bh₃ molecule," Phys. Rev. A 5, 50–67 (1972).
- ⁶³T. D. Crawford and H. F. Schaefer, "An Introduction to Coupled Cluster Theory for Computational Chemists," in *Reviews in Computational Chemistry* (John Wiley & Sons, Ltd, 2000) pp. 33–136.

- ⁶⁴P. Piecuch, K. Kowalski, I. S. O. Pimienta, and M. J. Mcguire, "Recent advances in electronic structure theory: Method of moments of coupledcluster equations and renormalized coupled-cluster approaches," Int. Rev. Phys. Chem. 21, 527–655 (2002).
- ⁶⁵R. J. Bartlett and M. Musiał, "Coupled-cluster theory in quantum chemistry," Rev. Mod. Phys. **79**, 291–352 (2007).
- ⁶⁶I. Shavitt and R. J. Bartlett, *Many-Body Methods in Chemistry and Physics:* MBPT and Coupled-Cluster Theory, Cambridge Molecular Science (Cambridge University Press, Cambridge, 2009).
- ⁶⁷J. Tölle, "Fully analytic g0w0 nuclear gradients," J. Phys. Chem. Lett. 16, 3672–3678 (2025).
- ⁶⁸M. Lazzeri, C. Attaccalite, L. Wirtz, and F. Mauri, "Impact of the electronelectron correlation on phonon dispersion: Failure of Ida and gga dft functionals in graphene and graphite," Phys. Rev. B 78, 081406 (2008).
- ⁶⁹C. Faber, J. L. Janssen, M. Côté, E. Runge, and X. Blase, "Electron-phonon coupling in the c₆₀ fullerene within the many-body gw approach," Phys. Rev. B 84, 155104 (2011).
- ⁷⁰C. Faber, P. Boulanger, C. Attaccalite, E. Cannuccia, I. Duchemin, T. Deutsch, and X. Blase, "Exploring approximations to the gw self-energy ionic gradients," Phys. Rev. B 91, 155109 (2015).
- ⁷¹B. Monserrat, "Correlation effects on electron-phonon coupling in semiconductors: Many-body theory along thermal lines," Phys. Rev. B 93, 100301 (2016)
- ⁷²Z. Li, G. Antonius, M. Wu, F. H. da Jornada, and S. G. Louie, "Electron-phonon coupling from ab initio linear-response theory within the *gw* method: Correlation-enhanced interactions and superconductivity in $ba_{1-x}k_xbio_3$," Phys. Rev. Lett. **122**, 186402 (2019).
- ⁷³Z. Li, G. Antonius, Y.-H. Chan, and S. G. Louie, "Electron-phonon coupling from gw perturbation theory: Practical workflow combining berkeleygw, abinit, and epw," Comp. Phys. Comm. 295, 109003 (2024).
- ⁷⁴E. E. Salpeter and H. A. Bethe, "A relativistic equation for bound-state problems," Phys. Rev. 84, 1232 (1951).
- ⁷⁵G. Strinati, "Application of the Green's functions method to the study of the optical properties of semiconductors," Riv. Nuovo Cimento 11, 1–86 (1988).
- ⁷⁶S. Ismail-Beigi and S. G. Louie, "Excited-state forces within a first-principles green's function formalism," Phys. Rev. Lett. 90, 076401 (2003).
- ⁷⁷M. S. Kaczmarski, Y. Ma, and M. Rohlfing, "Diabatic states of a photoexcited retinal chromophore from ab initio many-body perturbation theory," Phys. Rev. B 81, 115433 (2010).
- ⁷⁸O. Çaylak and B. Baumeier, "Excited-state geometry optimization of small molecules with many-body green's functions theory," J. Chem. Theory Comput. 17, 879–888 (2021).
- ⁷⁹I. Knysh, I. Duchemin, X. Blase, and D. M. Jacquemin, "Modelling of excited state potential energy surfaces with the bethe-salpeter equation formalism: The 4-(dimethylamino)benzonitrile twist," J. Chem. Phys. 157, 194102 (2022).
- ⁸⁰J. Villalobos-Castro, I. Knysh, D. Jacquemin, I. Duchemin, and X. Blase, "Lagrangian z-vector approach to bethe–salpeter analytic gradients: Assessing approximations," J. Chem. Phys. 159, 024116 (2023).
- 81 I. Knysh, J. D. Villalobos-Castro, I. Duchemin, X. Blase, and D. Jacquemin, "Exploring bethe–salpeter excited-state dipoles: The challenging case of increasingly long push–pull oligomers," J. Phys. Chem. Lett. 14, 3727–3734 (2023).
- ⁸²I. Knysh, K. Letellier, I. Duchemin, X. Blase, and D. Jacquemin, "Excited state potential energy surfaces of n-phenylpyrrole upon twisting: reference values and comparison between bse/gw and td-dft," Phys. Chem. Chem. Phys. 25, 8376–8385 (2023).
- ⁸³ J. Tölle, M.-P. Kitsaras, and P.-F. Loos, "Fully analytic nuclear gradients for the bethe–salpeter equation," J. Phys. Chem. Lett. 16, 11134–11143 (2025).
- ⁸⁴X. Blase, I. Duchemin, and D. Jacquemin, "The bethe–salpeter equation in chemistry: relations with td-dft, applications and challenges," Chem. Soc. Rev. 47, 1022–1043 (2018).
- ⁸⁵X. Blase, I. Duchemin, D. Jacquemin, and P.-F. Loos, "The bethe–salpeter equation formalism: From physics to chemistry," J. Phys. Chem. Lett. 11, 7371–7382 (2020).
- ⁸⁶W. Kutzelnigg, "Quantum chemistry in Fock space. I. The universal wave and energy operators," J. Chem. Phys. 77, 3081–3097 (1982).
- ⁸⁷W. Kutzelnigg and S. Koch, "Quantum chemistry in Fock space. II. Effective

- Hamiltonians in Fock space," J. Chem. Phys. 79, 4315–4335 (1983).
- ⁸⁸W. Kutzelnigg, "Quantum chemistry in Fock space. III. Particle-hole formalism," J. Chem. Phys. 80, 822–830 (1984).
- ⁸⁹R. J. Bartlett, S. A. Kucharski, and J. Noga, "Alternative coupled-cluster ansätze II. The unitary coupled-cluster method," Chem. Phys. Lett. 155, 133–140 (1989).
- ⁹⁰P. G. Szalay, M. Nooijen, and R. J. Bartlett, "Alternative ansätze in single reference coupled-cluster theory. III. A critical analysis of different methods," J. Chem. Phys. 103, 281–298 (1995).
- ⁹¹ A. G. Taube and R. J. Bartlett, "New perspectives on unitary coupled-cluster theory," Int. J. Quantum Chem. **106**, 3393–3401 (2006).
- ⁹²W. Kutzelnigg, "Unconventional Aspects of Coupled-Cluster Theory," in *Recent Progress in Coupled Cluster Methods: Theory and Applications*, Challenges and Advances in Computational Chemistry and Physics, edited by P. Cársky, J. Paldus, and J. Pittner (Springer Netherlands, Dordrecht, 2010) pp. 299–356.
- ⁹³T. C. Berkelbach, "Communication: Random-phase approximation excitation energies from approximate equation-of-motion coupled-cluster doubles," J. Chem. Phys. **149**, 041103 (2018).
- ⁹⁴D. Bohm and D. Pines, "A collective description of electron interactions. i. magnetic interactions," Phys. Rev. 82, 625–634 (1951).
- ⁹⁵D. Pines and D. Bohm, "A collective description of electron interactions: Ii. collective vs individual particle aspects of the interactions," Phys. Rev. 85, 338–353 (1952).
- ⁹⁶D. Bohm and D. Pines, "A collective description of electron interactions: Iii. coulomb interactions in a degenerate electron gas," Phys. Rev. **92**, 609–625 (1953).
- ⁹⁷P. Nozières and D. Pines, "Correlation energy of a free electron gas," Phys. Rev. 111, 442–454 (1958).
- ⁹⁸P. Ring and P. Schuck, *The Nuclear Many-Body Problem* (Springer, 2004).
- ⁹⁹G. P. Chen, V. K. Voora, M. M. Agee, S. G. Balasubramani, and F. Furche, "Random-phase approximation methods," Annu. Rev. Phys. Chem. 68, 421– 445 (2017).
- ¹⁰⁰X. Ren, N. Marom, F. Caruso, M. Scheffler, and P. Rinke, "Beyond the G W approximation: A second-order screened exchange correction," Phys. Rev. B 92, 081104 (2015).
- ¹⁰¹M. S. Hybertsen and S. G. Louie, "Electron correlation in semiconductors and insulators: Band gaps and quasiparticle energies," Phys. Rev. B 34, 5390–5413 (1986).
- ¹⁰²M. Shishkin and G. Kresse, "Self-consistent \$GW\$ calculations for semi-conductors and insulators," Phys. Rev. B 75, 235102 (2007).
- ¹⁰³X. Blase and C. Attaccalite, "Charge-transfer excitations in molecular donor-acceptor complexes within the many-body bethe-salpeter approach," Appl. Phys. Lett. 99, 171909 (2011).
- ¹⁰⁴C. Faber, C. Attaccalite, V. Olevano, E. Runge, and X. Blase, "First-principles GW calculations for DNA and RNA nucleobases," Phys. Rev. B 83, 115123 (2011).
- ¹⁰⁵T. Rangel, S. M. Hamed, F. Bruneval, and J. B. Neaton, "Evaluating the gw approximation with ccsd(t) for charged excitations across the oligoacenes," J. Chem. Theory Comput. 12, 2834–2842 (2016).
- ¹⁰⁶X. Gui, C. Holzer, and W. Klopper, "Accuracy assessment of gw starting points for calculating molecular excitation energies using the bethe–salpeter formalism," J. Chem. Theory Comput. 14, 2127–2136 (2018).
- ¹⁰⁷S. V. Faleev, M. van Schilfgaarde, and T. Kotani, "All-Electron Self-Consistent G W Approximation: Application to Si, MnO, and NiO," Phys. Rev. Lett. 93, 126406 (2004).
- ¹⁰⁸M. van Schilfgaarde, T. Kotani, and S. Faleev, "Quasiparticle Self-Consistent G W Theory," Phys. Rev. Lett. 96, 226402 (2006).
- ¹⁰⁹T. Kotani, M. van Schilfgaarde, and S. V. Faleev, "Quasiparticle self-consistent G W method: A basis for the independent-particle approximation," Phys. Rev. B 76, 165106 (2007).
- ¹¹⁰S.-H. Ke, "All-electron gw methods implemented in molecular orbital space: Ionization energy and electron affinity of conjugated molecules," Phys. Rev. B 84, 205415 (2011).
- ¹¹¹F. Kaplan, M. E. Harding, C. Seiler, F. Weigend, F. Evers, and M. J. van Setten, "Quasi-Particle Self-Consistent GW for Molecules," J. Chem. Theory Comput. 12, 2528–2541 (2016).
- ¹¹²A. Marie and P.-F. Loos, "A Similarity Renormalization Group Approach to Green's Function Methods," J. Chem. Theory Comput. 19, 3943–3957 (2023).

- ¹¹³G. Strinati, H. J. Mattausch, and W. Hanke, "Dynamical correlation effects on the quasiparticle bloch states of a covalent crystal," Phys. Rev. Lett. 45, 290–294 (1980).
- ¹¹⁴M. S. Hybertsen and S. G. Louie, "First-Principles Theory of Quasiparticles: Calculation of Band Gaps in Semiconductors and Insulators," Phys. Rev. Lett. 55, 1418–1421 (1985).
- ¹¹⁵R. W. Godby, M. Schlüter, and L. J. Sham, "Self-energy operators and exchange-correlation potentials in semiconductors," Phys. Rev. B 37, 10159– 10175 (1988).
- ¹¹⁶W. von der Linden and P. Horsch, "Precise quasiparticle energies and hartree-fock bands of semiconductors and insulators," Phys. Rev. B 37, 8351–8362 (1988).
- ¹¹⁷J. E. Northrup, M. S. Hybertsen, and S. G. Louie, "Many-body calculation of the surface-state energies for si(111)2×1," Phys. Rev. Lett. 66, 500–503 (1991).
- ¹¹⁸X. Blase, X. Zhu, and S. G. Louie, "Self-energy effects on the surface-state energies of h-si(111)1×1," Phys. Rev. B **49**, 4973–4980 (1994).
- ¹¹⁹M. Rohlfing, P. Krüger, and J. Pollmann, "Efficient scheme for gw quasi-particle band-structure calculations with aapplications to bulk si and to the si(001)-(2×1) surface," Phys. Rev. B 52, 1905–1917 (1995).
- ¹²⁰ A. Klein, "Perturbation theory for an infinite medium of fermions. ii," Phys. Rev. 121, 950–956 (1961).
- ¹²¹J. M. Luttinger and J. C. Ward, "Ground-state energy of a many-fermion system. ii," Phys. Rev. 118, 1417–1427 (1960).
- ¹²²G. Baym and L. P. Kadanoff, "Conservation laws and correlation functions," Phys. Rev. 124, 287–299 (1961).
- ¹²³M. Potthoff, "Self-energy-functional approach to systems of correlated electrons," Eur. Phys. J. B 32, 429–436 (2003).
- ¹²⁴V. Galitskii and A. Migdal, Sov. Phys. JETP 7, 96 (1958).
- ¹²⁵B. Holm and F. Aryasetiawan, "Total energy from the Galitskii-Migdal formula using realistic spectral functions," Phys. Rev. B 62, 4858 (2000).
- ¹²⁶C.-O. Almbladh, U. V. Barth, and R. V. Leeuwen, "Variational total energies from Φ-and Ψ-derivable theories," Int. J. Mod. Phys. B 13, 535–541 (1999).
- ¹²⁷N. E. Dahlen and U. von Barth, "Variational energy functionals tested on atoms," Phys. Rev. B 69, 195102 (2004).
- ¹²⁸N. E. Dahlen and U. von Barth, "Variational second-order Møller–Plesset theory based on the Luttinger–Ward functional," J. Chem. Phys. 120, 6826– 6831 (2004).
- ¹²⁹N. E. Dahlen and R. van Leeuwen, "Self-consistent solution of the Dyson equation for atoms and molecules within a conserving approximation," J. Chem. Phys. 122, 164102 (2005).
- ¹³⁰N. E. Dahlen, R. Van Leeuwen, and U. Von Barth, "Variational energy functionals of the Green function tested on molecules," Int. J. Quantum Chem. 101, 512–519 (2005).
- ¹³¹N. E. Dahlen, R. van Leeuwen, and U. von Barth, "Variational energy functionals of the Green function and of the density tested on molecules," Phys. Rev. A 73, 012511 (2006).
- ¹³² A. Stan, N. E. Dahlen, and R. van Leeuwen, "Fully self-consistent *GW* calculations for atoms and molecules," Europhys. Lett. EPL **76**, 298–304 (2006).
- ¹³³A. Stan, N. E. Dahlen, and R. van Leeuwen, "Levels of self-consistency in the GW approximation," J. Chem. Phys. 130, 114105 (2009).
- ¹³⁴S. Ismail-Beigi, "Correlation energy functional within the gw-RPA: Exact forms, approximate forms, and challenges," Phys. Rev. B 81, 195126 (2010).
- ¹³⁵M. E. Casida, "Time-dependent density functional response theory for molecules," (World Scientific, Singapore, 1995) pp. 155–192.
- ¹³⁶K. Sawada, "Correlation energy of an electron gas at high density," Phys. Rev. 106, 372–383 (1957).
- ¹³⁷K. Sawada, K. A. Brueckner, N. Fukuda, and R. Brout, "Correlation energy of an electron gas at high density: Plasma oscillations," Phys. Rev. 108, 507–514 (1957).
- ¹³⁸D. J. Rowe, "Methods for calculating ground-state correlations of vibrational nuclei," Phys. Rev. 175, 1283 (1968).
- ¹³⁹D. L. Freeman, "Coupled-cluster expansion applied to the electron gas: Inclusion of ring and exchange effects," Phys. Rev. B 15, 5512–5521 (1977).
- ¹⁴⁰G. E. Scuseria, T. M. Henderson, and D. C. Sorensen, "The ground state correlation energy of the random phase approximation from a ring coupled cluster doubles approach," J. Chem. Phys. 129, 231101 (2008).
- ¹⁴¹G. Jansen, R.-F. Liu, and J. G. Ángyán, "On the equivalence of ring-coupled

- cluster and adiabatic connection fluctuation-dissipation theorem random phase approximation correlation energy expressions," J. Chem. Phys. 133, 154106 (2010).
- ¹⁴²G. E. Scuseria, T. M. Henderson, and I. W. Bulik, "Particle-particle and quasiparticle random phase approximations: Connections to coupled cluster theory," J. Chem. Phys. 139, 104113 (2013).
- ¹⁴³D. Peng, S. N. Steinmann, H. van Aggelen, and W. Yang, "Equivalence of particle-particle random phase approximation correlation energy and ladder-coupled-cluster doubles," J. Chem. Phys. 139, 104112 (2013).
- ¹⁴⁴V. Rishi, A. Perera, and R. J. Bartlett, "A route to improving rpa excitation energies through its connection to equation-of-motion coupled cluster theory," J. Chem. Phys. 153, 234101 (2020).
- ¹⁴⁵J. Gauss, "Molecular properties," in *Modern Methods and Algorithms of Quantum Chemistry*, edited by J. Grotendorst (John von Neumann Institute for Computing, 2000) pp. 541–592.
- ¹⁴⁶T. Helgaker, P. Jørgensen, and J. Olsen, *Molecular Electronic-Structure Theory* (John Wiley & Sons, Inc., 2013).
- ¹⁴⁷J. Rekkedal, S. Coriani, M. F. Iozzi, A. M. Teale, T. Helgaker, and T. B. Pedersen, "Communication: Analytic gradients in the random-phase approximation," J. Chem. Phys. 139, 81101 (2013).
- ¹⁴⁸J. F. Stanton and R. J. Bartlett, "The equation of motion coupled-cluster method. a systematic biorthogonal approach to molecular excitation energies, transition probabilities, and excited state properties," J. Chem. Phys. 98, 7029–7039 (1993).
- ¹⁴⁹S. V. Levchenko, T. Wang, and A. I. Krylov, "Analytic gradients for the spin-conserving and spin-flipping equation-of-motion coupled-cluster models with single and double substitutions," J. Chem. Phys. 122, 224106 (2005).
- ¹⁵⁰S. Kvaal, "Variational formulations of the coupled-cluster method in quantum chemistry," Mol. Phys. 111, 1100–1108 (2013).
- ¹⁵¹C. Holzer, A. M. Teale, F. Hampe, S. Stopkowicz, T. Helgaker, and W. Klopper, "Gw quasiparticle energies of atoms in strong magnetic fields," J. Chem. Phys. 150, 214112 (2019).
- ¹⁵²J. Arponen, "Variational principles and linked-cluster exp s expansions for static and dynamic many-body problems," Ann. Phys. 151, 311–382 (1983).
- ¹⁵³J. Arponen, "The method of stationary cluster amplitudes and the phase transition in the lipkin pseudospin model," J.Phys. G: Nuc. Phys. 8, L129– L134 (1982).
- ¹⁵⁴J. S. Arponen, R. F. Bishop, and E. Pajanne, "Extended coupled-cluster method. i. generalized coherent bosonization as a mapping of quantum theory into classical hamiltonian mechanics," Phys. Rev. A 36, 2519–2538 (1987).
- ¹⁵⁵J. S. Arponen, R. F. Bishop, and E. Pajanne, "Extended coupled-cluster method. ii. excited states and generalized random-phase approximation," Phys. Rev. A 36, 2539–2549 (1987).
- ¹⁵⁶S. J. Bintrim and T. C. Berkelbach, "Full-frequency gw without frequency," J. Chem. Phys. 154, 041101 (2021).
- 157 M.-P. Kitsaras, Finite magnetic-field Coupled-Cluster methods: Efficiency and Utilities, Ph.D. thesis, Johannes-Gutenberg Universität Mainz (2023).
- ¹⁵⁸F. Hampe, S. Stopkowicz, N. Groß, M.-P. Kitsaras, L. Grazioli, S. Blaschke, L. Monzel, U. P. Yergün, and C.-M. Röper, "Qcumbre, quantum chemical utility enabling magnetic-field dependent investigations benefitting from rigorous electron-correlation treatment," Https://www.qcumbre.org/.
- ¹⁵⁹J. Gauss, F. Lipparini, S. Burger, S. Blaschke, M.-P. Kitsaras, T. Nottoli, J. Oswald, S. Stopkowicz, and T. Uhlířová, "MINT, Mainz INTegral package," (2015-2025), Johannes Gutenberg-Universität Mainz, unpublished.

- ¹⁶⁰D. A. Matthews, L. Cheng, M. E. Harding, F. Lipparini, S. Stopkowicz, T.-C. Jagau, P. G. Szalay, J. Gauss, and J. F. Stanton, "Coupled-cluster techniques for computational chemistry: The cfour program package," J. Chem. Phys. 152, 214108 (2020).
- ¹⁶¹J. F. Stanton, J. Gauss, L. Cheng, M. E. Harding, D. A. Matthews, and P. G. Szalay, "CFOUR, Coupled-Cluster techniques for Computational Chemistry, a quantum-chemical program package," With contributions from A. Asthana, A.A. Auer, R.J. Bartlett, U. Benedikt, C. Berger, D.E. Bernholdt, S. Blaschke, Y. J. Bomble, S. Burger, O. Christiansen, D. Datta, F. Engel, R. Faber, J. Greiner, M. Heckert, O. Heun, M. Hilgenberg, C. Huber, T.-C. Jagau, D. Jonsson, J. Jusélius, T. Kirsch, M.-P. Kitsaras, K. Klein, G.M. Kopper, W.J. Lauderdale, F. Lipparini, J. Liu, T. Metzroth, L.A. Mück, D.P. O'Neill, T. Nottoli, J. Oswald, D.R. Price, E. Prochnow, C. Puzzarini, K. Ruud, F. Schiffmann, W. Schwalbach, C. Simmons, S. Stopkowicz, A. Tajti, T. Uhlířová, J. Vázquez, F. Wang, J.D. Watts, P. Yergün. C. Zhang, X. Zheng, and the integral packages MOLECULE (J. Almlöf and P.R. Taylor), PROPS (P.R. Taylor), ABACUS (T. Helgaker, H.J. Aa. Jensen, P. Jørgensen, and J. Olsen), and ECP routines by A. V. Mitin and C. van Wüllen. For the current version, see http://www.cfour.de.
- ¹⁶²P. F. Loos, "QuAcK: a software for emerging quantum electronic structure methods," (2019), https://github.com/pfloos/QuAcK.
- ¹⁶³P. F. Loos, B. Pradines, A. Scemama, E. Giner, and J. Toulouse, "A density-based basis-set incompleteness correction for gw methods," J. Chem. Theory Comput. 16, 1018–1028 (2020).
- ¹⁶⁴J. F. Stanton and J. Gauss, "A simple scheme for the direct calculation of ionization potentials with coupled-cluster theory that exploits established excitation energy methods," J. Chem. Phys. 111, 8785–8788 (1999).
- ¹⁶⁵T. H. Dunning, "Gaussian basis sets for use in correlated molecular calculations. i. the atoms boron through neon and hydrogen," J. Chem. Phys. 90, 1007–1023 (1989).
- ¹⁶⁶R. A. Kendall, T. H. Dunning, and R. J. Harrison, "Electron affinities of the first-row atoms revisited. systematic basis sets and wave functions," J. Chem. Phys. 96, 6796–6806 (1992).
- ¹⁶⁷B. P. Prascher, D. E. Woon, K. A. Peterson, T. H. Dunning, and A. K. Wilson, "Gaussian basis sets for use in correlated molecular calculations. vii. valence, core-valence, and scalar relativistic basis sets for li, be, na, and mg," Theor. Chem. Acc. 128, 69–82 (2011).
- ¹⁶⁸D. E. Woon and T. H. Dunning, "Gaussian basis sets for use in correlated molecular calculations. iii. the atoms aluminum through argon," J. Chem. Phys. 98, 1358–1371 (1993).
- ¹⁶⁹W. Nelson, P. Bokes, P. Rinke, and R. W. Godby, "Self-interaction in Green's-function theory of the hydrogen atom," Phys. Rev. A 75, 032505 (2007).
- ¹⁷⁰P. Romaniello, S. Guyot, and L. Reining, "The Self-Energy beyond GW: Local and Nonlocal Vertex Corrections," J. Chem. Phys. 131, 154111 (2009).
- ¹⁷¹F. Aryasetiawan, R. Sakuma, and K. Karlsson, "GW Approximation with Self-Screening Correction," Phys. Rev. B 85, 035106 (2012).
- ¹⁷²J. Wetherell, M. J. P. Hodgson, and R. W. Godby, "gw self-screening error and its correction using a local density functional," Phys. Rev. B **97**, 121102 (2018)
- ¹⁷³Š. Budzák, G. Scalmani, and D. Jacquemin, "Accurate Excited-State Geometries: a CASPT2 and Coupled-Cluster Reference Database for Small Molecules," J. Chem. Theory Comput. 13, 6237–6252 (2017).
- ¹⁷⁴P.-F. Loos, M. Boggio-Pasqua, A. Blondel, F. Lipparini, and D. Jacquemin, "Quest database of highly-accurate excitation energies," J. Chem. Theory Comput. 21, 8010–8033 (2025).